Royal Netherlands Institute for Sea Research

Utrecht University

MSc Thesis

Particulate trace metal dynamics in the Amundsen Sea Polynya, the Southern Ocean

Flora Wille
37.5 ECTS
August 2019 - April 2020

Department of Ocean Systems, Royal Netherlands Institute for Sea Research (NIOZ)
Department of Earth Sciences, Utrecht University (UU)

First supervisor: Prof. Dr. Gert-Jan Reichart (UU/NIOZ)
Second supervisor: Dr. Rob Middag (NIOZ)
Daily supervisor: Mathijs van Manen, MSc (NIOZ)

Abstract

The Southern Ocean plays an important role in the global biogeochemical cycling of elements and the uptake of anthropogenic CO_2. Due to climate change, the Southern Ocean is experiencing rapid melt of ice shelves and glaciers, which may have fundamental effects on the biogeochemistry and closely related carbon pump. The Amundsen Sea Polynya (ASP) is the most productive polynya per unit area in the Southern Ocean and can be studied as a model region for the effects of increased glacial melt. This study analysed the particulate trace metal distributions of Mn, Fe, Co, Ni, Cu and Zn in the ASP and how these link to particulate trace metal sources. Particulate trace metal distributions were studied along a transect that follows the intrusion of warm and saline Circumpolar Deep Water (CDW) onto the shelf through a trough that leads to the Dotson Ice Shelf (DIS), where the CDW intrudes into the sub-ice shelf cavities and causes ice shelf thinning and basal melt. Concentrations of both labile and refractory fractions were analysed to assess the potential bioavailability of the particulate suspended matter in the ASP. Biogenic and lithogenic contributions were calculated to assess the composition of the particulate trace metal pool. These show that particulate Mn and particulate Fe only have minor biogenic contributions and mainly consist of lithogenic material that includes both crustal, sedimentary and likely additional authigenic phases. The results showed that atmospheric dust input and sea ice melt were only minor sources of particulate trace metals, and likely contribute very little to sustaining the immense phytoplankton bloom that occurs annually in the ASP. The outflow of meltwater from the DIS however, was highly enriched in both labile and refractory particulate trace metals, notably particulate Fe and Mn. This is the first study to show that the outflow of meltwater from beneath the DIS supplies large quantities of labile particulate Mn and Fe to the ASP, which are assumed to be potentially bioavailable within days. The predicted increase in ice shelf and basal melt due to climate change would thus likely increase the flux of (labile) particulate trace metals to the ASP, and therefore has the potential to increase primary productivity and atmospheric CO_2 uptake. Consequently, increased basal melt and ice shelf thinning might create a small negative feedback on global climate change.

Table of Contents

1. Introduction

Oceans play an important role in regulating global climate change and have absorbed roughly a third of anthropogenic CO_2 emissions (Sabine et al., 2004). The rate of carbon sequestration in the oceans partly relies on the efficiency of the physical and biological pump in high latitude seas, as these are areas of deep water formation where carbon is transported to the deep seas. High latitude oceans therefore influence long term trends in atmospheric CO_2 concentrations (Sigman & Boyle, 2000). The Southern Ocean, that encircles Antarctica, is a particularly crucial player in this process. It has been estimated to be responsible for 40 percent of marine anthropogenic CO_2 uptake, despite constituting only 6% of the total oceans area (Frölicher et al., 2015; Khatiwala et al., 2009; Mikaloff Fletcher et al., 2006). The Southern Ocean furthermore supplies nutrients to low latitude oceans, which influences the magnitude of biological productivity in these oceans (Sarmiento et al., 2004). The Southern Ocean and Antarctica are experiencing high melt rates due to ocean warming (e.g. Rignot et al., 2013), which could have fundamental effects on the biogeochemistry and physical processes that link to carbon sequestration. Despite the Southern Ocean being subjected to rapid climate change and being globally important to the biogeochemical cycling of elements and uptake of anthropogenic CO_2, there is a lack of observational constraints, which lead to large uncertainties in climate modelling studies. Recent studies (e.g. Landschützer et al., 2015) have suggested that the Southern Ocean CO_2 sink is sensitive to climate variability and more variable than previously thought. This highlights the importance of fully understanding the biogeochemical and physical processes governing the Southern Ocean.

The Southern Ocean is the largest High Nutrient Low Chlorophyll (HNLC) region of the world's oceans. In HNLC regions, phytoplankton biomass is lower than expected based on the ample supply of the major nutrients nitrogen, phosphorous and silicate. In the Southern Ocean HNLC region, primary production is mainly limited by light and the micronutrient and trace metal iron (e.g. Martin, 1990; Martin et al., 1990a; Mitchell and Holm-Hansen, 1991; de Baar et al., 1995; Sunda and Huntsman, 1997). There are however regions of exceptionally high productivity in Antarctic shelf waters; so-called polynyas (Arrigo and van Dijken, 2003). Polynyas are annually recurring areas of open water surrounded by sea ice at locations where sea ice would be expected based on climatological conditions. Polynyas are often highly biologically productive since they are the first open water areas to be exposed to the increasing solar irradiance during springtime and are often located near micronutrient sources (Arrigo et al., 2003, 2015). According to satellite data, the most productive polynya per unit area in the Southern Ocean is the Amundsen Sea Polynya (ASP). The mean Chlorophyll *a* concentration, an indicator of phytoplankton biomass, is highest in the ASP during the spring bloom with a value of 2.28 mg m^{-3} with respect to an average of 0.6 mg m^{-3} in all Antarctic polynyas (Arrigo et al., 2015*)*.

The ASP is located in the Amundsen Sea in western Antarctica (Figure 1). Besides the ASP, the Amundsen Sea also contains a smaller and slightly less productive polynya, the Pine Island Polynya (PIP) *(*Arrigo and Van Dijken, 2003, 2015). The ASP opens annually in austral spring and summer (Arrigo and Van Dijken, 2003, 2015). The open water generally increases from 10,000 m^2 in December to a maximum extent of 60,000 m^2 in February and decreases to less than 10,000 m^2 by late March. Inter annual variability is high however (Arrigo et al., 2012). Primary productivity increases from November onwards as sea ice melts and the open water area expands. Peak productivity is observed in December and early January. From mid-January onwards the phytoplankton bloom gradually decreases (Arrigo et al., 2012).

The Amundsen Sea is characterized by perennial sea ice and is surrounded by several large outlet glaciers that terminate in floating ice shelves such as the Crosson, Dotson and Getz Ice Shelves (Figure 1). Relatively warm and saline Circumpolar Deep Water that originates from the Antarctic Circumpolar Current flows through troughs towards the ice shelves at the coast (section 2; Figure 2). At the coast, it flows into the sub-ice cavities of the ice shelves causing ice shelf thinning and basal melt (e.g. Walker et al., 2007; Wåhlin et al., 2010; Arneborg et al., 2012). The Amundsen Sea experiences some of the most rapid melting rates and ice sheet thinning of the Southern Ocean (e.g. Jacobs et al., 2011; Jenkins et al., 2010; Rignot et al., 2008, 2014) and the ASP is subject to some of the highest basal melt rates in all Antarctic polynyas (Arrigo et al., 2015; Rignot et al., 2013).

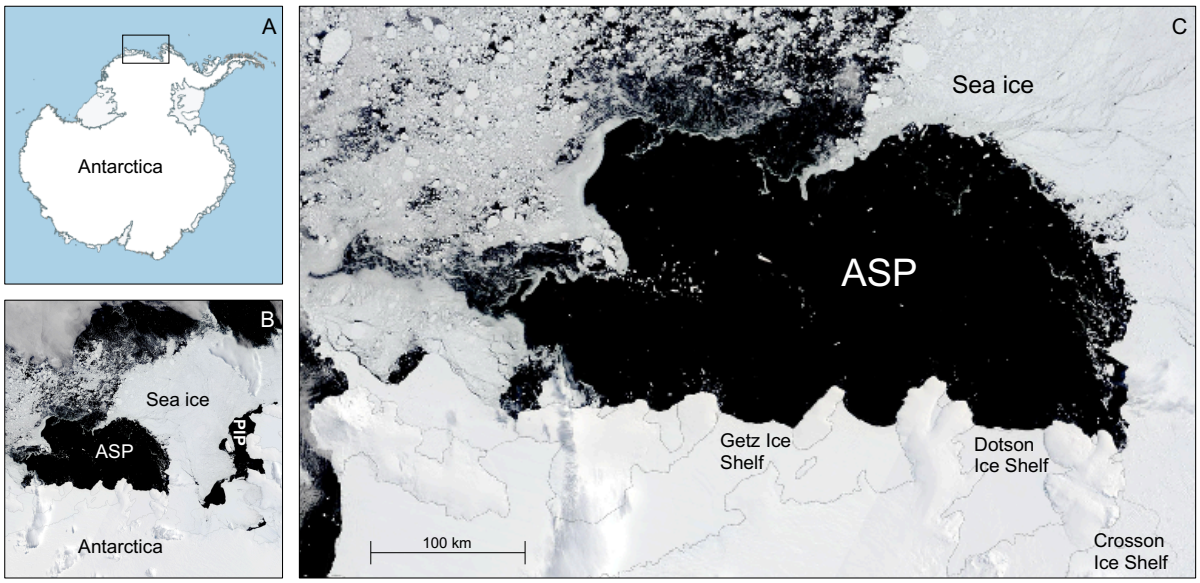

Figure 1. (A) Location of the Amundsen Sea in Antarctica; (B) Amundsen Sea with the locations of the Amundsen Sea Polynya (ASP) and Pine Island Polynya (PIP); (C) ASP with the Crosson, Dotson and Getz Ice Shelves; (B-C) Moderate Resolution Imaging Spectroradiometer (Terra/MODIS) true colour satellite images from January 10, 2018 (source: NASA Worldview).

Glacial meltwater input can influence stratification and trace metal distributions. Phytoplankton require a series of bio-essential trace metals for cellular functions and processes, such as cofactors in metalloenzymes (Sunda, 1989), nitrogen fixation, chlorophyll synthesis and electron transport chains of photosynthesis and respiration (Twining et al., 2013). Phytoplankton require the following bio-essential trace metals (in order of cellular abundance); iron (Fe), zinc (Zn), manganese (Mn), copper (Cu), nickel (Ni) and cobalt (Co) (De Baar et al., 2017). Alteration of trace metal distributions due to increased glacial meltwater input can therefore influence the biogeochemistry, primary productivity and phytoplankton community composition of the area. This could have implications for the functioning of the biological pump of the region, which in turn plays a role in anthropogenic CO_2 uptake (Arrigo et al., 2008b). It is therefore imperative to understand trace metal cycling and distributions in the Amundsen Sea, how these link to biogeochemical dynamics and physical processes, and how this could change in the future.

There have been relatively few studies on biogeochemical trace metal dynamics in the Amundsen Sea due to the inaccessibility and remoteness of the region. It takes two weeks to reach the Amundsen Sea by ship from the nearest port and the area is perennially surrounded by sea ice, which makes field campaigns expensive and logistically hard to organise. The studies performed to date have focussed mainly on dissolved trace metals, operationally defined as the fraction that passes through a 0.2µm pore size filter. Specific interest has been on Fe (Alderkamp et al., 2012, 2015; Gerringa et al., 2012; Sherrell et al., 2015). Gerringa et al. (2012) showed that dissolved and total dissolvable Fe from glacial melt are the main sources that fuel phytoplankton blooms in the Amundsen Sea. They mainly focussed on the PIP and sampled relatively few stations in the ASP. Recent modelling studies support findings that glacial melt plays an important role in supplying Fe to the ASP (St-Laurent et al., 2017, 2019). A more rigorous sampling campaign was carried out during the 2010-2011 Amundsen Sea Polynya International Research Expedition (ASPIRE; Yager et al., 2012). Alderkamp et al. (2015) and Sherrell et al. (2015) reported on Fe and other trace metal findings of the ASPIRE cruise. Alderkamp et al. (2015) studied the effects of Fe and light availability in bioassay experiments and suggest that a higher Fe availability, possibly due to higher melt rates in the future, would increase photosynthesis rates and water column productivity. Sherrell et al. (2015) studied the distribution and dynamics of dissolved Fe and other bioactive trace metals (Mn, Ni, Cu and Zn) in the ASP. They showed that the distributions of these trace metals suggest that the accelerated basal melt of the ice shelves in the ASP, caused by inflow of warm CDW underneath the ice shelves, plays a critical role in providing the Fe flux needed to maintain the intense phytoplankton bloom in the ASP.

In contrast to the relatively large interest in dissolved trace metals, studies on particulate trace metals in the Amundsen Sea are scarce. This despite particulate trace metals often exceeding dissolved concentrations and likely being part of and a source to the bioavailable trace metal pool (e.g. Gerringa et al., 2012; Hurst et al., 2010). The particulate trace metal fraction is defined as the fraction that does not pass through a 0.45µm pore size filter. Particulate trace metals are associated with suspended particulate matter such as phytoplankton cells, detrital particles, authigenic minerals, crustal particles and suspended sediments. Particles can be both sources and sinks for trace metals by processes such as dissolution, remineralization, scavenging and biological uptake and therefore play an important role in trace metal cycling (Goldberg, 1954; Turekian, 1977). To date, only Planquette et al. (2013) have focussed on particulate trace metals in the Amundsen Sea, with again, a primary focus on Fe. Planquette et al. (2013) analysed concentrations of total particulate Fe, Al, Mn and P. Sampling was done in the ASP, PIP and ice-covered waters surrounding these polynyas. The ASP was sparsely sampled, only at ice shelf fronts. The study shows that the influence of lithogenic particles dominates in the water column. The elemental composition and spatial distribution of the particulate trace metals suggest that sediment resuspension and ice shelf melt mainly govern the supply of particulate Fe to the Amundsen Sea and that these sources potentially support the phytoplankton bloom in the ASP.

This study presents particulate trace metal distributions of the bio-essential particulate trace metals Fe, Mn, Co, Ni, Cu and Zn in the ASP in the austral summer of 2017/2018. The sampled transect follows a similar transect to the dissolved trace metal study of Sherrell et al. (2015). This study complements the particulate trace metal findings in the Amundsen Sea of Planquette et al. (2013) by providing data across the ASP that is not solely limited to the ice shelf fronts. Furthermore, the potential bioavailability of the particulate trace metal pool was assessed by analysing two fractions; labile and refractory fractions. The aim of this study is to understand the particulate trace metal dynamics in the ASP, how these link to trace metal sources and accompanying processes, and how these might change in the future.

2. Regional setting and hydrography

Glacial melt, ice shelf thinning and sediment resuspension caused by intrusion of CDW have been hypothesized to be an important source of trace metals to the ASP and therefore sustain phytoplankton blooms in the Amundsen Sea (e.g. Gerringa et al., 2012; Planquette et al., 2013; Alderkamp et al., 2015; Sherrell et al., 2015). The regional bathymetry and hydrography are thus important factors to consider in context of trace metal distributions.

The ASP is located on the Amundsen Sea continental shelf, which is situated south of 71°S between 100°W and 135°W (Figure 1; Nitsche et al., 2007). The shelf is characterized by several deep throughs that bisect the shelf and deepen in landward direction (Figure 2). These troughs connect to present day ice shelves and glacier systems and were carved during past glaciations when grounded ice reached the shelf edge (Evans et al., 2006; Nitsche et al., 2007). The Dotson Trough bisects the shelf at the precise location where the ASP is located and finds its origin in three deep sub-troughs, which are connected to the Dotson and Getz Ice Shelves and their sub-ice cavities (Figure 2). Relatively warm and saline Circumpolar Deep Water (CDW) that originates from the Antarctic Circumpolar Current (ACC) intrudes onto the Amundsen Sea continental shelf via the Dotson Through (Figure 2; Walker et al., 2007). The intruding CDW is the densest water mass on the shelf, causing it to flow at the bottom of the Dotson Trough and intrude into the sub-ice shelf cavities beneath the Dotson Shelf where it causes basal melt and ice shelf thinning (e.g. Walker et al., 2007; Wåhlin et al., 2010; Arneborg et al., 2012). Inflow of CDW beneath the Dotson Ice Shelf (DIS) occurs on the eastern side of the trough and outflow occurs on the western side of the trough (e.g. Wåhlin et al., 2013). The intruding CDW is modified (mCDW) by cooling and freshening due to mixing with colder surface layers and glacial melt water beneath the ice shelves.

There are generally three typical water masses present in the Amundsen Sea; CDW(mCDW), Winter Water (WW) and Antarctic Surface Water (ASSW). WW is a cold and saline water mass formed as a product of sea ice formation and generally lies on top of the warm and dense CDW. ASSW is surface water that is seasonally warmed by solar radiation and freshened by sea ice melt. The ASSW is therefore relatively warm and fresh compared to the other water masses present. Naturally, mixing occurs, causing a vague boundary between the water masses. Properties of the water masses are not fixed due to varying degrees of warming, sea ice melt, mixing, etc. In this study CDW is therefore defined as the warmest most saline water mass, WW is defined as the coldest most saline water mass and ASSW is defined as the warmest and freshest water mass.

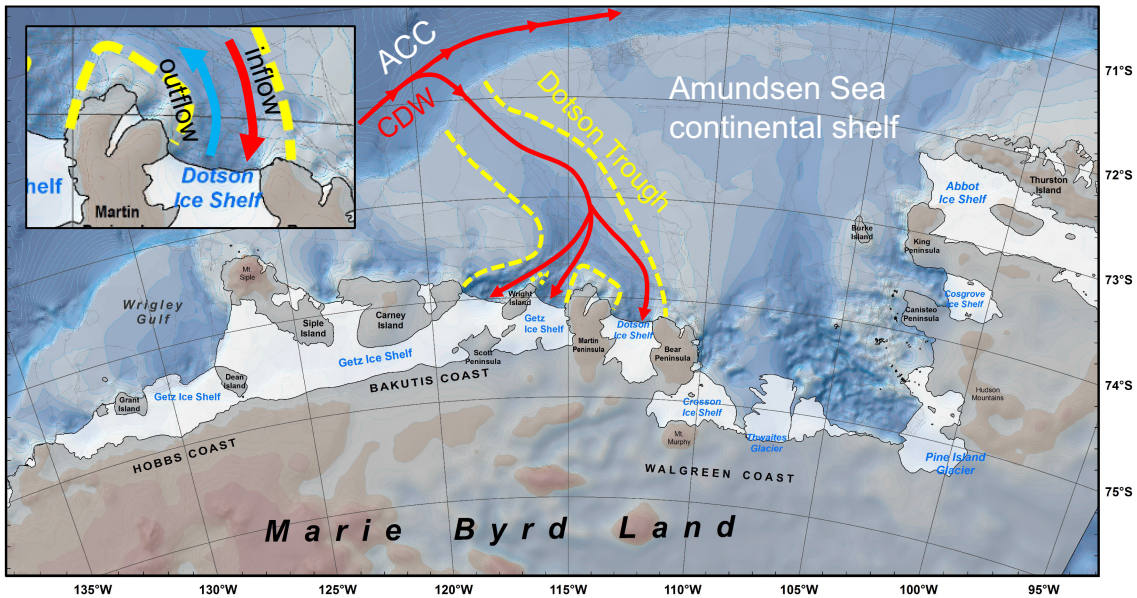

Figure 2. Bathymetry map of the Amundsen Sea continental shelf with Dotson Trough indicated by yellow dashed lines and inflow of CDW onto the shelf indicated by red arrows. Inflow of CDW into the Dotson Ice Shelf cavities and consequent outflow are represented by blue and red arrows in the upper left corner. Figure is adapted from Nitsche et al. (2007).

3. Materials and Methods

3.1 Study site

Samples were collected onboard the South Korean icebreaker RV Araon during the ANA08B research expedition to the Amundsen Sea in the austral summer of 2017/2018. The sampling period spanned from the 24th of January to the 30th of January 2018. The ASP was completely surrounded by sea ice at the start of the sampling campaign, whereas the polynya had started to open to the open ocean on the north west side at the end of sampling (Figure 3B, 3C). Samples were taken along a transect that follows the in- and outflow of CDW through the Dotson Trough (Figure 3A). Of this transect, station 53 was located off the shelf and outside the polynya in the marginal sea ice zone, station 52 was located near the outermost edge of the polynya, stations 42 and 36 were located at the DIS front on the in -and outflow side respectively, and the remaining stations were located in the central open water body of the ASP (Figure 3A).

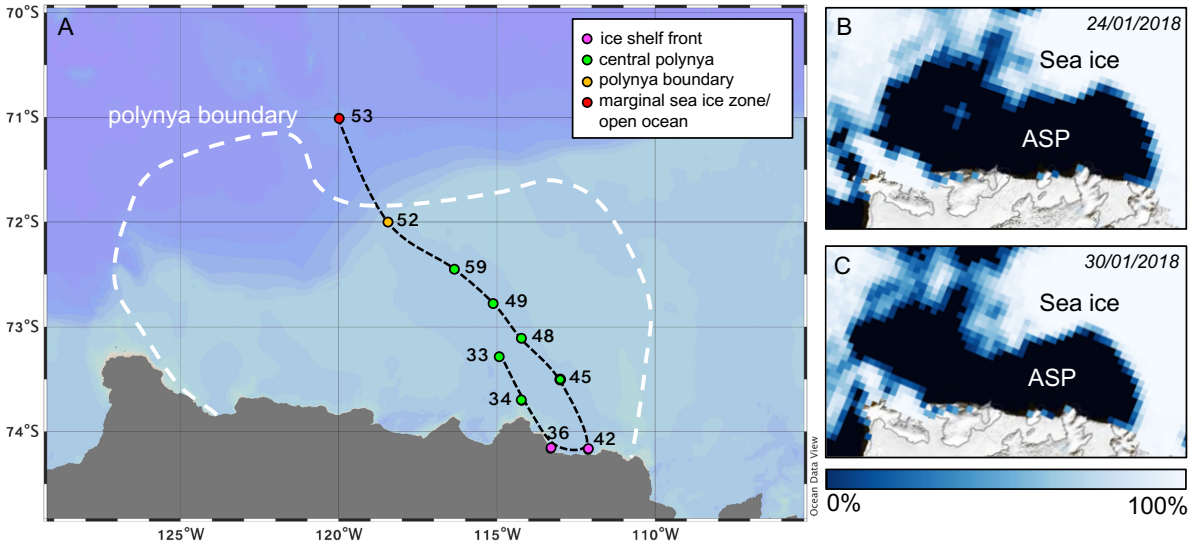

Figure 3. (A) Bathymetric map of the study area with the cruise transect (black dashed line), trace metal sampled stations (coloured dots) and approximate outline of the polynya (white dashed line); (B) Percentage sea ice concentration at the start of sampling and (C) at the end of sampling; (B-C) 12km spatial resolution Advanced Microwave Scanning Radiometer-E/Advanced Microwave Scanning Radiometer-2 (AMSR-E/AMSR2) images (source: NASA Worldview).

3.2 Sample collection

Each station consisted of CTD (conductivity, temperature, depth) measurements and additional sampling of seawater for particulate trace metal analysis at 6 to 11 depths per station. The stations were sampled with an all titanium ultra clean CTD sampling system for trace metals equipped with polyvinylidene fluoride (PVDF) samplers (De Baar et al., 2008; Rijkenberg et al., 2015). Immediately after recovery, the CTD system was moved into a cleanroom environment in a modified high cube shipping container (ISO class 5). Temperature inside the container was near ambient seawater temperature. Unfiltered seawater samples were collected in 10L, acid cleaned, carboys (VWR Collection) and stored in dark plastic bags until the moment of filtration. Before the cruise, 25 mm poly-ether-sulfone (PES) disc filters (0.45 µm Pall Supor) were cleaned by heating the filters at 60°C for 24h in 3x sub-boiled distilled 1.2M HCl (VWR Chemicals – AnalaR NORMAPUR) and rinsing them 5 times with MQ water (18.2 MΩ). Filters were stored in MQ water (18.2 MΩ) until use. Filtrations were done within a maximum of two hours after sampling. Before the start of the filtrations, samples were gently homogenized and the filters were placed in polypropylene (PP) filter holders (Advantec). Filter holders were placed on the caps (Nalgene) of the carboys using PP luer-locks (Cole-Palmer). Carboys were then hung upside down onto the CTD frame using a custom-made PP carboy frame. Filtration was done under nitrogen gas pressure (0.5 bar overpressure). Samples were filtered for a maximum of two hours and checked regularly for leaks. After filtration excess seawater was removed by gentle air pressure. The filters were removed from the filter holders and were stored frozen (-20°C) in plastic bags until analysis.

3.3 Sample digestion

The particulate trace metal filters were subjected to two consecutive digestion protocols to determine labile and refractory fractions. All vials used in the digestion procedures were rigorously cleaned before and between use by rinsing the vials 5 times with MQ water (18.2 MΩ), refluxing them in 3x sub-boiled distilled 7M HCl (VWR Chemicals – AnalaR NORMAPUR®) on a hotplate at 110°C for a minimum of 12 hours, and rinsing the vials 5 times with MQ again before use. All actions were conducted in a laminar flow cabinet (ISO class 5), except for refluxing, drying and all steps involving HF, which were done in a regular fume hood equipped with a heating block (EasyDigest®). Drying steps were performed in a closed environment (EvapoClean®) and refluxing was done in closed vials to prevent atmospheric exchange. Both the laminar flow cabinet and fume hood were placed in a clean lab (ISO class 8).

3.3.1 Labile particulate fraction

To solubilize the labile fraction of the particulate trace metal samples, the filters were subjected to a leach initially developed by Chester and Hughes (1967), further modified and developed by Berger et al. (2008) and evaluated by Rauschenberg and Twining (2015). Filters were placed in cleaned 2 mL Eppendorf vials to which a solution of 1.8 mL of 4.35M (25%) 2x sub-boiled distilled acetic acid and 0.02M (2%) hydroxylamine hydrochloride (Sigma-Aldrich – 99.999% trace metal basis) was added. The vials were heated to 95°C for 10 minutes in a water bath and were subsequently cooled down to room temperature. After being in contact with the leach solution for a total of 2 hours, the filters were moved to 30 mL Teflon vials (Savillex) and processed for refractory elements (section 3.3.2). The remaining leachate was centrifuged at 16,000 RCF for 10 minutes to bring any remaining particles to the bottom of the solution in the Eppendorf vials. Next, 1.6 mL of leachate was transferred to separate 30 mL Teflon vials (Savillex) without disturbing any remaining particles in the Eppendorf vials and 100 µL of concentrated HNO_3 was added. The vials were then heated to dryness at 110°C. The dried vial contents were re-dissolved in 2mL 1.5% 3x sub-boiled distilled HNO_3 (10 ppb Rh internal standard), refluxed at 110°C for 30 minutes and transferred to 2mL Cryovials® for storage and subsequent analysis. These samples represent the labile fraction.

3.3.2 Refractory particulate fraction

Refractory elements were digested following a total digestion protocol developed by Cullen and Sherrell (1999) and further modified by Planquette and Sherrell (2012). The remaining 0.2 mL of leachate and particles in the Eppendorf® vials from the previous step (section 3.3.1) were transferred to the Teflon vials already containing the filters (section 3.3.1). To these vials, 2mL of a solution of 3x sub-boiled distilled 8.0M (50%) HNO_3 (VWR Chemicals – AnalaR NORMAPUR) and 2.9M (10%) HF (Merck - Supelco) was added. The vials were closed tightly and refluxed for 4 hours at 110°C. The filters did not remain adhered to the walls of the vials and were visibly altered by digestion, but still intact. Afterwards, the vials were cooled, and the contents were poured into secondary Teflon vials (Savillex) without transferring the filters. The original digestion vials were thoroughly rinsed with MQ water (18.2 MΩ) to ensure complete transfer of sample. This was also poured into the secondary Teflon vials and the filters were discarded. The secondary Teflon vials were then heated to dryness at 110°C. To the dried vial contents, 1 mL of a solution of 8.0M (50%) 3x sub-boiled distilled HNO_3 (VWR Chemicals – AnalaR NORMAPUR) and 15% H_2O_2 (Merck – Suprapur) was added. The vials were refluxed for 1 hour at 110°C and subsequently cooled to room temperature. Adding reagent and refluxing were repeated once, after which the vials were heated to dryness at 110°C. The samples were redissolved in 2 mL 1.5% 3x sub-boiled distilled HNO_3 (10 ppb Rh internal standard) and transferred to 2 mL Cryovials® for storage and analysis. These samples represent the refractory fraction.

3.3.3 Blanks

Three types of blanks were analysed to determine the average background trace metal concentration of the different components in the digestion procedure; acid blanks, filter blanks and process blanks. Acid blanks simply consisted of digestion acids. These blanks were treated identically to the particulate trace metal samples, except for the steps involving filter handling and removal. Filter blanks consisted of new acid cleaned filters that had not been in contact with seawater. Filter blanks were also treated and analysed identically to the particulate trace metal filter samples. Process blanks consisted of filters that were treated

identically to the particulate trace metal filters, but instead of filtering unfiltered sea water, seawater that had previously been filtered over a 0.2mm filter cartridge (Sartobran-300, Sartorius) was filtered. Process blanks were analysed identically to the particulate trace metal filter samples. All blanks were corrected for outliers by omitting values that did not fall within ± 2SD of the blank average. Particulate trace metal samples were corrected for filter blank values, see section 5.1. Blanks values are reported in section 4.1.

3.3.4 Certified Reference Materials

Accuracy and precision of the digestions were assessed by Certified Reference Materials (CRMs). There is no available CRM for marine suspended particulate matter, therefore accuracy could only be approximated by analysis of other available CRMs. For this study BCR-414 (freshwater phytoplankton, certified by the Community Bureau of Reference, European Commission's Joint Research Centre), PACS-2 and MESS-3 (marine sediments, National Research Council of Canada) were analysed. For each CRM 10-30 mg was digested. The recommended sample weights are however 100 mg for BCR-414 and 250 mg for PACS-2 and MESS-3. The lower sample weights in this study were chosen to be representative of actual marine particulate suspended matter concentrations (similar to Ohnemus et al., 2014). BCR-414 was subjected to the consecutive labile leach and refractory total digestion and solely the total digestion. PACS-2 and MESS-3 were only subjected to the total digestion. The CRMs were digested identically to the particulate filter samples (sections 3.3.1 and 3.3.2). CRM values are reported in section 4.2.

3.4 Sample analysis

Particulate trace metal samples, blanks and CRMs were analysed by Inductively Coupled Plasma – Mass Spectrometry (Thermo Scientific Sector Field High Resolution Element 2) at the Royal Netherlands Institute for Sea Research (NIOZ). The introduction system consisted of a micro sampler with a perfluoroalkoxy (PFA) nebulizer and had a sample introduction rate of 55 µL/min. The instrument was equipped with Standard H Nickel cones. The isotopes Cd-111 and Pb-208 were analysed in low resolution. All other isotopes were measured in medium resolution. A 5- and 6-point standard addition series, for P and other elements respectively, were measured at the beginning of each run for quantification of sample concentrations. To correct for changes in instrumental sensitivity during analysis, Rh-103 was used as internal standard. Drift standards were measured after every block of 13 samples to correct for drift during the runs. Final concentrations were calculated from Rh-normalized and drift corrected values.

4. Results

4.1 Blanks

For both the labile leach and refractory digestion, acid blanks generally have the lowest values, followed by filter blanks and process blanks respectively (Table 1). There are a few exceptions however; P has a lower refractory filter blank than acid blank and Fe has a slightly lower labile filter blank than acid blank. Other elements such as Co, Ni and Cu have slightly higher, but fairly similar values for the labile filter blanks with respect to labile acid blanks. For all elements, process blanks are evidently the highest blank values. For the elements P, Mn and Fe the process blanks are as much as ~20-100 times higher than the acid and filter blanks for both the labile leach and refractory digestion.

Whether the labile leach or refractory digestion has a higher blank value depends mostly on the elements considered; Mn, Ni, Cu and Zn have higher values for the labile leach than for the refractory digestion for all blank types. Similarly, Al and Fe have higher values for the labile leach for both the acid and filter blanks, but lower values for the process blanks. The element P has higher values for the labile leach for the filter and process blanks, but lower values for the acid blank. In contrast to the majority of the other elements, Ti has higher refractory values for all blank types. Labile and refractory blank values for each blank type and element are generally not more than 1 to 6 times greater than the lower value (either labile or refractory). Remarkably, Ti has refractory blank values that are between 24 and 65 times higher than the labile blanks values.

Acid, filter and process blanks all have high standard deviations due to a large spread in blank values. Some standard deviations are nearly equal to or even exceed the average blank value, for instance the standard deviations of the labile and refractory acid blanks for Zn and the standard deviation of the refractory acid blank for P. The implications of these large standard deviations and other trends in blank values as presented here, are discussed in section 5.1.

Table 1. Acid, filter and process blanks (pmol/vial) of the labile leach (labile), subsequent total digestion (refractory) and separate total digestion (total). See appendix A for an overview of blanks for all analysed elements.

	Al	P	Ti	Mn	Fe	Co	Ni	Cu	Zn
Acid blank									
Labile	288.88	55.91	1.02	0.99	42.69	0.22	13.09	3.60	128.10
± 1SD	210.40	26.77	0.51	0.53	26.42	0.09	6.24	2.67	171.75
Refractory	205.46	174.70	25.99	0.34	15.93	0.29	7.91	1.42	34.43
± 1SD	33.30	213.91	7.19	0.19	9.42	0.17	2.09	0.46	40.00
Total	206.54	73.38	33.75	0.25	9.17	0.23	7.90	11.94	22.28
± 1SD	12.83	9.77	10.35	0.05	2.30	0.22	0.34	21.40	18.68
Filter blank									
Labile	358.56	93.34	2.88	1.39	42.48	0.27	15.86	3.64	223.07
± 1SD	145.98	80.97	2.52	0.26	9.63	0.08	6.99	2.02	83.94
Refractory	302.70	74.12	188.32	0.68	33.06	0.44	10.81	2.91	37.91
± 1SD	111.29	19.34	44.10	0.22	9.00	0.33	3.18	1.21	24.43
Process blank									
Labile	1389.56	3765.14	26.25	76.53	897.32	1.13	232.46	81.07	417.92
± 1SD	635.12	1425.37	14.73	50.17	462.01	0.07	209.52	31.34	190.73
Refractory	5434.07	1818.40	636.35	18.81	1815.97	0.57	14.98	23.41	65.87
± 1SD	3675.70	609.47	260.03	14.63	1123.07	0.41	10.82	8.13	5.00

4.2 Certified reference materials

All analysed CRM's have recovered concentrations that fall within the certified range or that are close to the certified range (Table 2). Recoveries of Fe for both the combined digest and separate total digest for BCR-414 fall within the certified range. The recovery of Ni for the combined digest similarly falls within the certified range. The other elements fall just outside the certified range, but have recoveries no lower than 86% and no higher than 106%. For BCR-414, recoveries are generally slightly higher for the separate total digest than for the combined labile leach and total digest. The marine sediment MESS-3 has recoveries that fall within the certified range for Al and Ti. The CRM PACS-2 has recoveries that fall within the certified range for P, Ti, Mn Co and Cu. Similar to BCR-414, the values that fall outside the certified ranges for MESS-3 and PACS-2 fall within 10 to 15 percent of the certified value. Standard deviations are lowest for BCR-414, varying between 1 and 5 percent of the average recovered value. MESS-3 and PACS-2 have higher standard deviations, varying between 10 and 15 percent of the average recovered value.

Table 2. Concentrations (µg/g; g/100g) and recoveries (%) of Certified Reference Materials ± 1SD. BCR-414 was analysed for the consecutive labile leach and total digestion (combined) and separate total digestion (total digest). MESS-3 and PACS-2 were solely subjected to the total digestion (total digest). Values are averages of triplicate samples.

	Al [g/100g]	P [g/100g]	Tl [g/100g]	Mn [µg/g]	Fe [g/100g]	Co [µg/g]	Ni [µg/g]	Cu [µg/g]	Zn [µg/g]
BCR-414									
Certified value	N/A	N/A	N/A	299 ± 13	1.85 ± 0.19[ab]	1.43 ± 0.06[a]	18.8 ± 0.8	29.5 ± 1.3	111.6 ± 2.5
Combined	-	-	-	258 ± 5	1.78 ± 0.043[b]	1.23 ± 0.016	18.6 ± 0.7	26.1 ± 0.4	101.3 ± 1.7
Recovery (%)	-	-	-	86 ± 2	96 ± 2	86 ± 1	99 ± 4	88 ± 1	91 ± 2
Total digest	-	-	-	267 ± 8	1.89 ± 0.049[b]	1.32 ± 0.07	19.9 ± 0.8	26.6 ± 0.8	106.5 ± 2.6
Recovery (%)	-	-	-	89 ± 3	102 ± 3	93 ± 5	106 ± 4	90 ± 3	95 ± 2
MESS-3									
Certified value	8.59 ± 0.23	0.12[a]	0.44 ± 0.06	324 ± 1	4.34 ± 0.11	14.4 ± 2.0	46.9 ± 2.2	33.9 ± 1.6	159 ± 8
Total digest	8.75 ± 1.16	0.11 ± 0.01	0.41 ± 0.05	302 ± 34	3.96 ± 0.51	12.3 ± 1.5	49.9 ± 9.1	29.3 ± 4.6	150 ± 20
Recovery (%)	102 ± 13	89 ± 10	93 ± 12	93± 11	91 ± 12	85 ± 11	106 ± 19	86 ± 14	94 ± 13
PACS-2									
Certified value	6.62 ± 0.32	0.096 ± 0.004	0.443 ± 0.032	440 ± 19	4.09 ± 0.06	11.5 ± 0.3	39.5 ± 2.3	310 ± 12	364 ± 23
Total digest	7.45 ± 0.73	0.097 ± 0.010	0.462 ± 0.048	442 ± 48	4.26 ± 0.46	11.3 ± 1.29	43.1 ± 4.5	310 ± 35	399 ± 56
Recovery (%)	113 ± 11	101 ± 10	104 ± 11	101 ± 11	104 ± 11	98 ± 11	109 ± 11	100 ±11	110 ± 15

[a] Only indicative value available.

[b] Concentrations in µg/g.

4.3 Water masses, fluorescence, oxygen and particulate P

To interpret the particulate trace metal distributions, a physical and biological context are required. Below, temperature and salinity data are presented and used to identify water masses. Fluorescence, oxygen and particulate phosphorus (pP) data are presented to give insight on the locations and scale of primary productivity in the ASP at the time of sampling.

4.3.1 Water masses

The temperature-salinity distribution (Figure 4) and temperature and salinity transect plots (Figure 4) illustrate that the three typical water masses of the ASP were present at the time of sampling (section 2). At the open ocean station (station 53), the relatively warm and saline CDW comprises almost the entire water column except for the approximate upper 150m (Figure 4). The intruding mCDW is present over the entire shelf up to the DIS front (station 42). Above the warm and saline mCDW intrusion, colder and less saline WW is present at all stations. Warm and relatively fresh AASW is present to maximum depths of approximately 100m. The coldest waters in the surface layer are located at the DIS front and at the open ocean station (station 53) and polynya boundary station (station 52). These stations are subjected to glacial meltwater input and sea ice melt respectively. The surface layer in the polynya has a slightly higher temperature than deeper waters as a result of warming by solar radiation. Similar to temperature, lowest salinities in the surface layer are found at the open ocean station (station 53) due to sea ice melt. This shallow decreased salinity layer extends further into the polynya (up to station 49). Salinities at the DIS front (station 42 and station 36) are not significantly lower due to mixing of meltwater with mCDW.

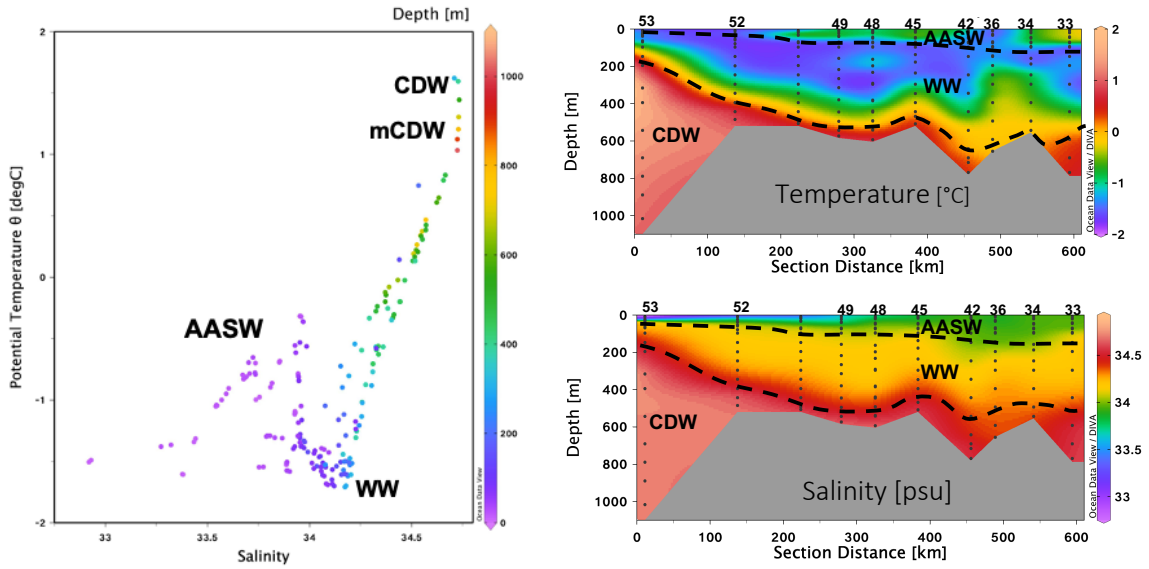

Figure 4. Potential temperature (°C) – Salinity (psu) diagram and transect plots of temperature (°C) and salinity (psu) along the sampled transect in the ASP. The T-S diagram shows the different water masses and respective depths of the samples in colour scale. Transect plots show the approximate locations of CDW, WW and AASW (black dashed lines).

4.3.2 Fluorescence and oxygen

The fluorescence sensor was not calibrated, so fluorescence values are in arbitrary units and values are only to be interpreted as a relative measurement. The fluorescence and dissolved oxygen concentrations roughly follow the same distribution over the water column (Figure 6). Highest fluorescence values are found in surface waters of the central polynya body stations (stations 33, 34, 45, 48, 49). Fluorescence values in the surface layer are lower at the ice shelf front stations (stations 42, 36), the open ocean station (station 53) and polynya boundary station (station 52). Surface oxygen concentrations are similar to the surface fluorescence distribution and are lower at the ice shelf front stations (stations 42, 36). In contrast to fluorescence, enhanced oxygen concentrations extend further to the boundary and outside the polynya (stations 52 and 53 respectively), but are constrained to a shallower surface layer. The oxygen distribution seems to match the intrusion of CDW onto the shelf (Figure 4), with lowest oxygen concentrations correlating with mCDW.

4.3.3 Particulate P

Labile and refractory pP distributions (Figure 7) resemble the fluorescence and oxygen distributions (Figure 6). The distributions of the labile and refractory fractions closely correlate with each other (r^2 = 0.96, $p<0.05$). Maximum concentrations are found in the upper 100m, followed by 100-fold lower concentrations for labile pP and 10-fold lower concentrations for refractory pP deeper in the water column. In the upper 100m, concentrations are highest in the polynya stations (stations 33, 34, 45, 48, 49, 52) and lowest in open ocean and sea ice station (station 53) and ice shelf front stations (stations 42, 36). Highest concentrations are present in the surface water of the polynya boundary (station 52). In the upper 100m, pP is largely present in the labile fraction. Deeper down in the water column there is less contrast between labile pP and refractory pP concentrations, with labile pP being only ~1-3 nM higher than refractory pP. Concentrations below 100m are generally <10nM and therefore neglibile compared to concentrations up to ~300 nM in the upper 100m.

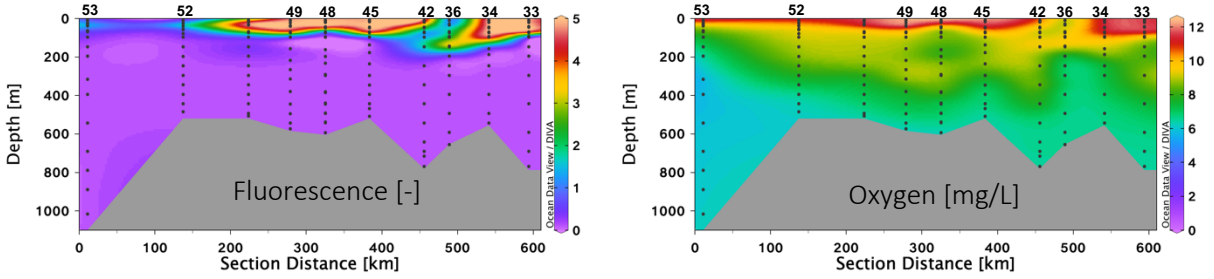

Figure 5. Fluorescence [-] and dissolved oxygen [mg/L] transect plots. Station numbers are presented above the figure and seafloor bathymetry is represented by grey areas.

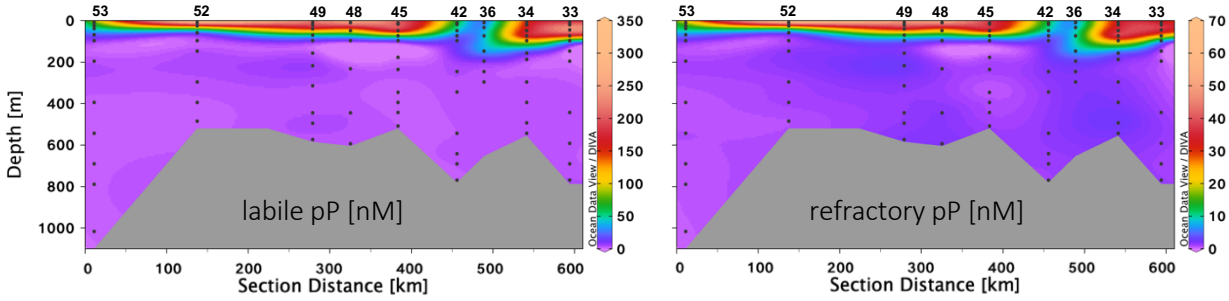

Figure 6. Labile pP [nM] and refractory pP [nM] distributions. Station numbers are presented above the figure and seafloor bathymetry is represented by grey areas.

4.4 Particulate trace metal distributions

The particulate trace metals are presented according to their distribution in the water column along the transect. First, the non-biological trace metals aluminium (Al) and titanium (Ti) are presented, followed by the bio-essential trace metals Mn, Fe, Co and Ni, Cu, Zn.

4.4.1 Particulate Al and Ti

Particulate Al (pAl) and particulate Ti (pTi) predominantly occur in the refractory fraction, with refractory concentrations being approximately 20-fold higher than labile concentrations (Figure 7). For both pAl and pTi the labile and refractory concentrations follow roughly the same distribution along the transect. Both labile and refractory fractions of pAl and pTi are significantly correlated ($p<0.05$). The highest concentrations are observed at the stations closest to the DIS front on the outflow side of the transect (stations 36 and 34). At these stations pAl and pTi have maximum concentrations at the same depths for both the labile and refractory fractions. Similarly, pAl and pTi both have higher concentrations at the central polynya body station 48, with maximum concentrations at the two lowermost sampled depths. The open ocean station (station 53) and polynya boundary station have the lowest pAl and pTi concentrations. At the open ocean station there is no observable trend with depth in the water column. The polynya boundary station however has increasing concentrations with depth in the water column.

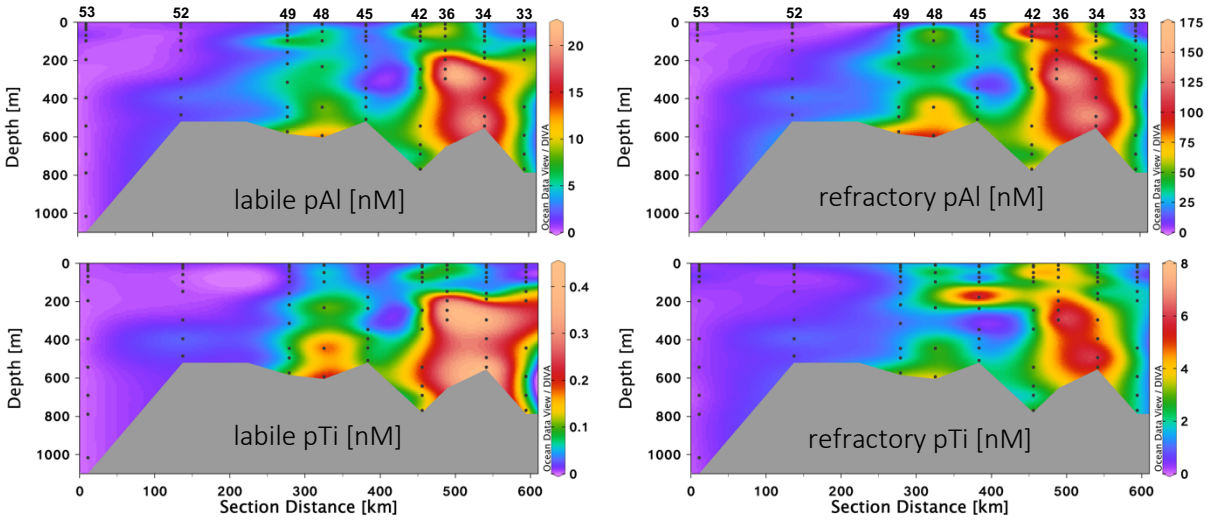

Figure 7. Labile pAl and pTi [nM] and refractory pAl and pTi [nM] distributions. Station numbers are presented above the figure and seafloor bathymetry is represented by grey areas.

4.4.2 *Particulate Mn, Fe and Co*

Particulate Mn (pMn), Fe (pFe) and Co (pCo) have similar distributions for both the labile and refractory fractions (Figure 8). The distributions resemble the pAl and pTi distributions, with highest concentrations at the stations closest to the DIS front on the outflow side (stations 36 and 34) and elevated concentrations at the central polynya body station 48. Labile and refractory pMn, pFe and pCo all correlate significantly with pAl and pTi ($p<0.05$). Labile pMn is present in slightly higher concentrations than refractory pMn, with ~4 times higher concentrations in the maxima at the outflow stations. In contrast, pFe has higher refractory concentrations, ~3 times higher refractory concentrations in the outflow stations. Similar to pMn, pCo is present in slightly higher labile concentrations. In the open ocean station (station 53), pMn, pFe and pCo concentrations do not have a trend with depth. At the polynya boundary station (station 52), both pMn and pFe have lower concentrations in the surface layer followed by higher concentrations deeper in the water column.

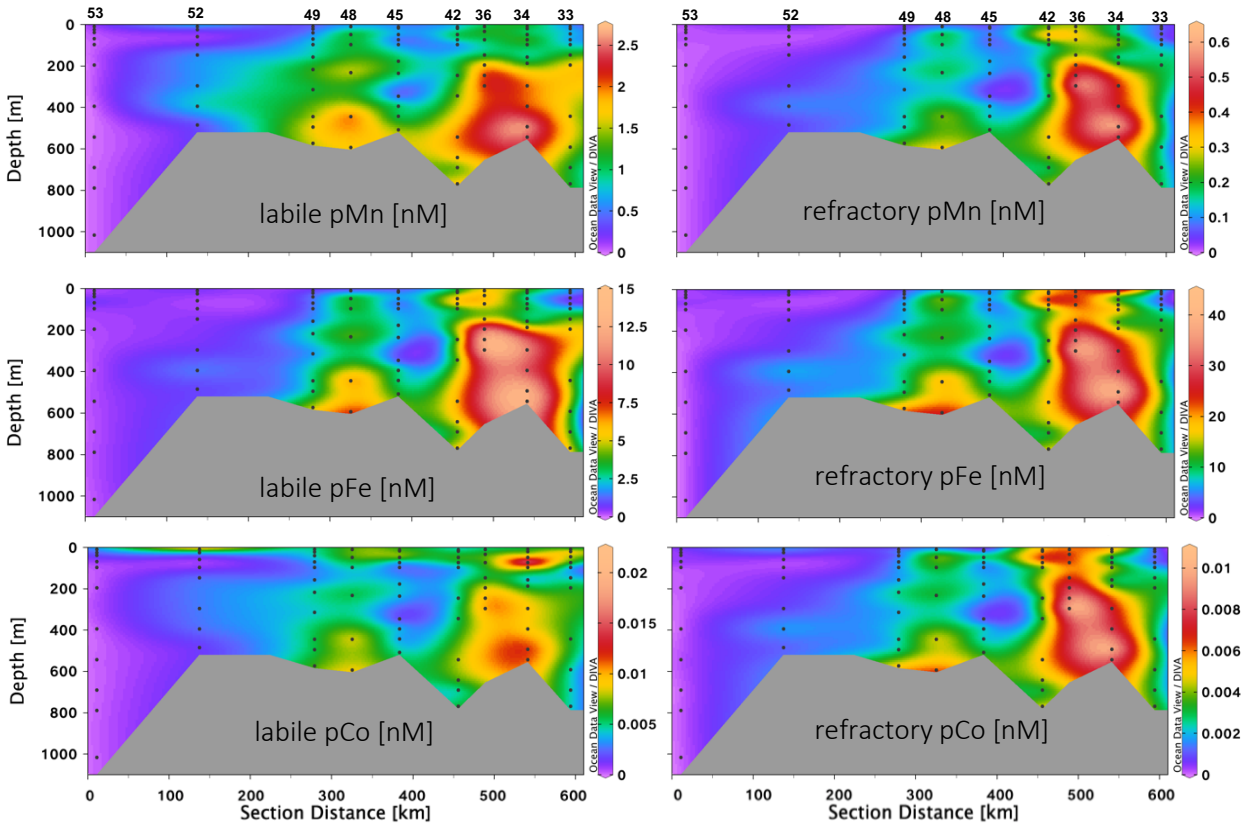

Figure 8. Labile pMn, pFe and pCo [nM] and refractory pMn, pFe, pCo [nM] distributions. Station numbers are presented above the figure and seafloor bathymetry is represented by grey areas.

4.4.3 *Particulate Ni, Cu and Zn*

Refractory particulate Ni (pNi) has a similar distribution to pAl and pTi (Figure 9), with higher concentrations at the ice shelf front outflow stations (station 36, 34). Labile pNi has highest concentrations in the upper 100m of the water column, as opposed to refractory pNi which has the highest concentrations below 100m. The labile pNi distribution is similar to the pP distribution and correlates well (r^2 = 0.82, p<0.05). Particulate Cu (pCu) also has highest concentrations in the upper 100m for both labile and refractory fractions (Figure 9), with slightly lower concentrations at the ice shelf front stations (stations 42 and 36). High surface pCu concentrations extend furthest down the water column in the central polynya body stations and are constrained to a shallower depth in the outer polynya edge station 52. Concentrations are lowest at the open ocean station (station 53), which has slightly elevated concentrations in the upper 100m and no significant trends deeper in the water column. Both labile and refractory pCu correlate well with pP (r^2 = 0.93, p<0.05; r^2 = 0.93, p<0.05). Labile particulate Zn (pZn) similarly correlates well with pP (r^2 = 0.87). Highest concentrations are found in the upper 100m with lower concentrations in the surface waters of the ice shelf front stations (Figure 9). In contrast, refractory pZn does not have a similar distribution to pP (p>0.05). There are no significant correlations with pAl and pTi either (p>0.05). Refractory pZn does have higher concentrations near the ice shelf front outflow stations (stations 36 and 34) deeper down in the water column and higher concentrations in the upper 100-200m of the central polynya stations (stations 45, 48, 49) and ice shelf front inflow station (station 42).

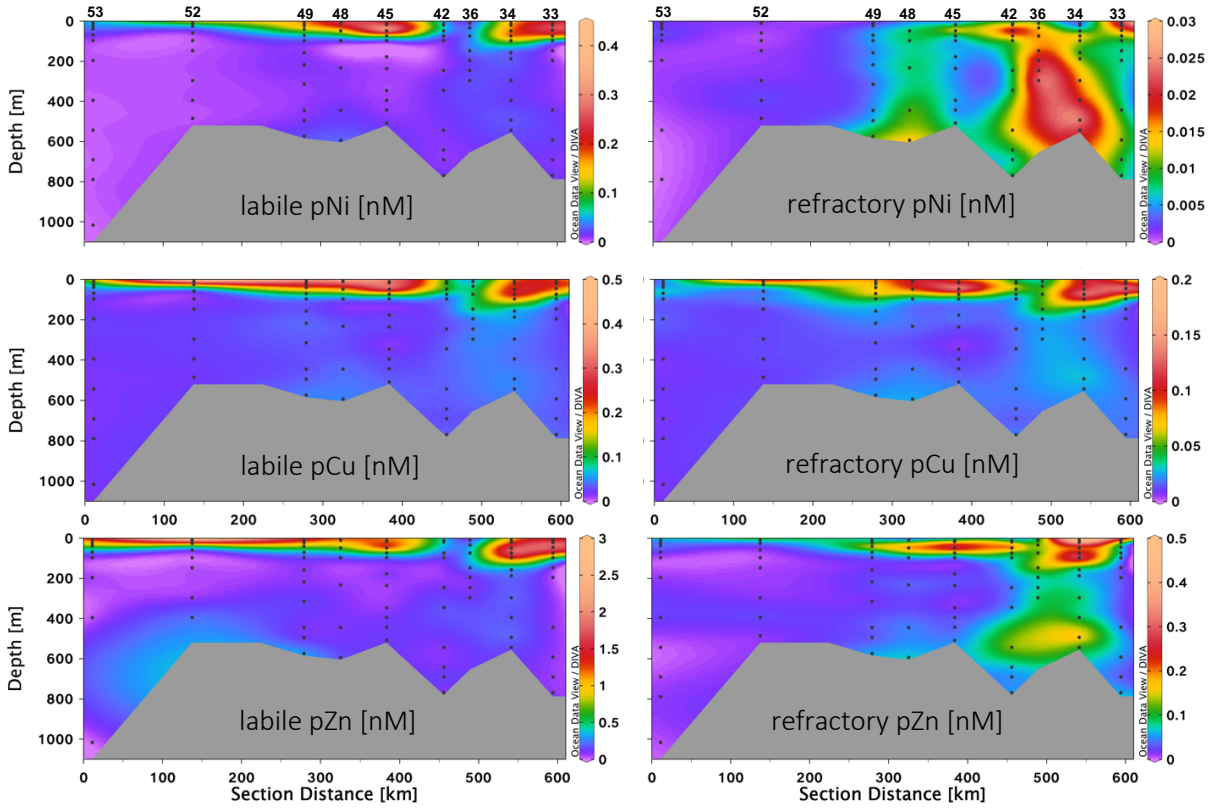

Figure 9. Labile pNi, pCu and pZn [nM] and refractory pNi, pCu and pZn [nM] distributions. Station numbers are presented above the figure and seafloor bathymetry is represented by grey areas.

5. Discussion

To understand the particulate trace metal dynamics in the ASP, it is imperative to understand the composition of the particulate trace metal pool and how this links to particulate trace metal sources and the accompanying processes that govern particulate trace metal distributions. It is in this context that the results of this study are discussed. The primary focus is put on pMn and pFe as these trace metals are most likely to be limiting phytoplankton growth in the ASP and the Southern Ocean.

5.1 Method evaluation

Particulate trace metal detection limits are determined by the elemental signal of the filter blank (Planquette and Sherrell, 2012). This poses a problem if the sample signal is of the same order of magnitude as the filter blank. As expected, filter blanks of this study were generally higher than acid blanks for both the labile leach and refractory digestion. There were a few instances where the acid blanks were higher or where the acid and filter blanks had similar values (section 4.1). This implies that, for some elements at least, the filter contribution to the total blank value is small (e.g. labile leach blanks for Co, Ni and Cu). The majority of elements do however have significantly higher filter blanks than acid blanks, implying that acid cleaned filters in most instances contribute significantly to the blank signal.

Planquette and Sherrell (2012) argued that more accurate filter blanks can be determined by filtering pre-filtered seawater through acid cleaned filters; so-called process blanks. They recommend extensive use of process blanks at multiple stations and depths along the sampling transect. The process blanks of this study have values that are of the same magnitude or even exceed sample signals. Process blanks were only taken at the ice shelf front outflow station (station 36). Concentrations of particulate trace metals were generally high at this station, causing the process blank to likely be unrepresentative for samples at locations with lower particulate trace metal concentrations. The high process blanks could be caused by dissolved trace metals absorbed onto the filters. Aggregation of colloids from the soluble phase in the pre filtered seawater could additionally cause high process blanks (Jensen et al., 2020). Since the process blanks overwhelmed sample signals for some samples, filter blanks were used for blank correction instead.

Acid and filter blank values of this study are in the same order of magnitude as the blank values found by previous studies (Rauschenberg and Twining, 2015; Ohnemus et al., 2014). Both Rauschenberg and Twining (2015) and Ohnemus et al. (2014) report high standard deviations, similar to the standard deviations of this study. This emphasizes that the filters and reagents used have highly variable trace metal signals and that the analytical procedure is susceptible to contamination. This does not pose a problem as long as sample signals are significantly higher than filter blank signals. For most elements the sample signal was indeed higher than the filter blank average. There were a few exceptions however, for instance there were samples where the filter blank values for labile Zn exceeded the sample signal, resulting in negative concentrations that were omitted. This emphasises the importance of maximum filter loading.

The CRM recoveries of this study fall within or are close to the certified range for all analysed CRMs. Ohnemus et al. (2014) and Planquette et al. (2013) show recoveries and standard deviations within similar ranges to this study. Standard deviations of MESS-3 and PACS-2 are slightly higher than the standard deviations of these CRMs in the before mentioned studies. It has to be noted that the masses of analysed CRMs are below the recommended sample weights. Furthermore, CRMs do not perfectly represent suspended particulate matter. They have no salt component and the marine sediment CRMs have a higher lithogenic component than suspended particulate matter (Ohnemus et al., 2014).

To summarize, blank values are variable and have high standard deviations, but are in the same order of magnitude as other studies. For most elements filter blank values were appropriate to correct the samples for blank values. Recoveries of CRMs were in or close to the certified range and are comparable to recoveries found by other studies. The analytical methods used are thus found to be adequate.

5.2 Particulate trace metal composition

In order to comprehend the sources and processes that govern particulate trace metal distributions in the ASP, it is imperative to first understand what kind of suspended particulate matter make up the particulate trace metal pool. Below, biogenic and lithogenic contributions are discussed.

5.2.1 Biogenic contribution

Biogenic particulate trace metals are defined as trace metals that are incorporated in or adsorbed onto biotic particles. Biotic particles include living phytoplankton cells (soft tissue and hard skeletal materials such as calcite and aragonite) and detritus (e.g. dead phytoplankton cells, fecal pellets). The particulate trace metal samples of this study were analysed for two subsequent fractions; the labile and refractory fractions. The labile fraction was extracted according to the leach described by Berger et al. (2008) and is defined as the fraction that consists of biogenic material and abiotic material that is available to phytoplankton on a short time frame (generations/days). The fraction includes living and dead phytoplankton cells, detritus and labile abiotic particles such as Fe, Mn and Al oxyhydroxides, Mn and Fe oxides, carbonates, and trace metals adsorbed onto the surface of alumino-silicate clay minerals (Berger et al., 2008). The remaining refractory fraction consists of insoluble trace metals incorporated in mineral lattices that are unavailable to phytoplankton on long time scales, such trace metals incorporated in crystalline oxyhydroxide minerals and alumino-silicate minerals (Berger et al., 2008).

According to the definition of the labile fraction by Berger et al. (2008), all biogenic material is extracted by the labile leach. Planquette et al. (2013) estimated the biogenic contribution to particulate trace metal concentrations by assuming all pP is of biogenic origin. Following this assumption, linear regression of labile pP with the labile particulate trace metal fractions indicates if there is a consistent biogenic component to the particulate trace metal pool. Fluorescence, oxygen and pP data show that primary productivity was restricted to the upper 100m of the water column (sections 4.3.2 and 4.3.3). For this reason, the upper 100m and deeper waters are assessed separately for biogenic contributions. Plotting labile particulate trace metals against labile pP and performing linear regression (Figure 11 and Figure 12) shows different trends for the upper 100m and deeper waters. Both pMn and pFe do not correlate with pP ($p>0.05$) throughout the water column. This indicates that there is no consistent biogenic pMn and pFe component and other types of labile particles likely dominate the pMn and pFe pools. The other labile particulate bio-essential trace metals do have significant trends with pP in the upper 100m. Here, pNi, pCu and pZn have strong correlations with pP (respectively $r^2=0.75$, $p<0.05$; $r^2=0.88$, $p<0.05$; $r^2=0.81$, $p<0.05$), pCo has a weaker but significant relationship with pP ($r^2=0.36$, $p<0.05$). The significant correlations imply that there is a consistent biogenic component in the upper 100m for these elements. The transect plots of labile pNi, pCu and pZn follow similar distributions to fluorescence, oxygen and pP (section 4), suggesting that these elements are indeed primarily dominated by biogenic material in the surface layer. Below 100m in the water column, only pNi and pCu have significant, though weak, relationships with pP (respectively $r^2=0.14$, $p<0.05$; $r^2=0.25$, $p<0.05$). The other trace metals all have non-significant relationships with pP (p-values >0.05). A potential explanation for this could be preferential mineralisation with respect to P of sinking biogenic detritus or that other sources of labile metals become more dominant at depth.

Planquette et al. (2013) quantified biogenic particulate trace metal contributions for total particulate Mn and Fe by multiplying Mn/P and Fe/P ratios with Southern Ocean diatom trace metal/P ratios published by Twining et al. (2004). Twining et al. (2004) analysed Mn, Fe, Ni and Zn in individual diatom cells for low Fe conditions (open ocean waters) and high Fe conditions (fertilized open ocean waters). The high Fe diatoms had a Mn/P ratio of 0.28 mmol mol^{-1}, Fe/P ratio of 1.93 mmol mol^{-1}, Ni/P ratio of 0.73 mmol mol^{-1} and Zn/P ratio of 6.2 mmol mol^{-1}. Following the procedure of Planquette et al. (2013), the percentage of biogenic trace metals of pMn, pFe, pNi and pZn were calculated (Appendix B1 and B2). The high Fe diatom ratios were used for the calculation, as the low Fe open Southern Ocean conditions are assumed to be unrepresentative of conditions in the ASP at time of sampling. It has to be noted that the calculation is a rough approximation since only diatom metal quotas are used. The phytoplankton community of the ASP has however been found to be spatially heterogeneous, with bloom-waters being dominated by the haptophyte *Phaeocystis antarctica* and non-bloom waters by diatoms (Alderkamp et al., 2012; Schofield et al., 2015). A more accurate estimation would thus include community averaged trace metal quotas,

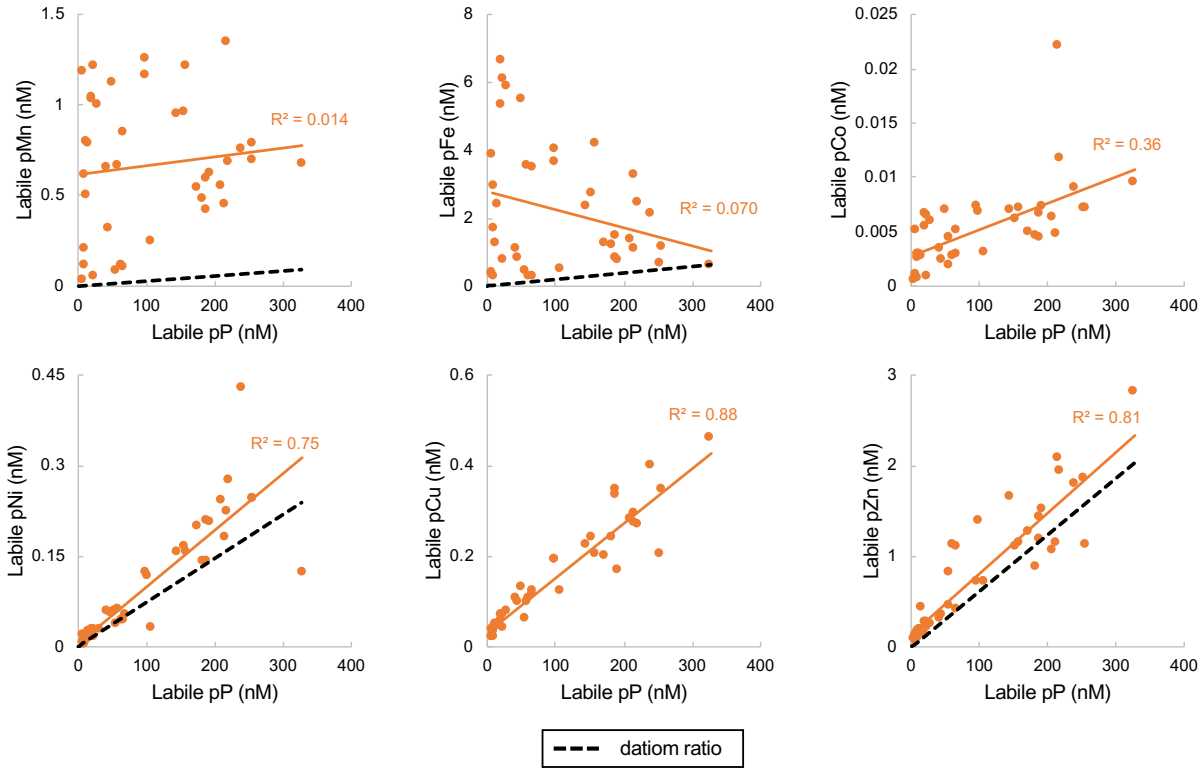

Figure 10. Labile pP (nM) plotted against labile pMn, pFe, pCo, pNi, pCu and pZn for samples <100m depth. Diatom ratios (Twining et al., 2004) are plotted for labile pMn, pFe, pNi and pZn (black dashed line).

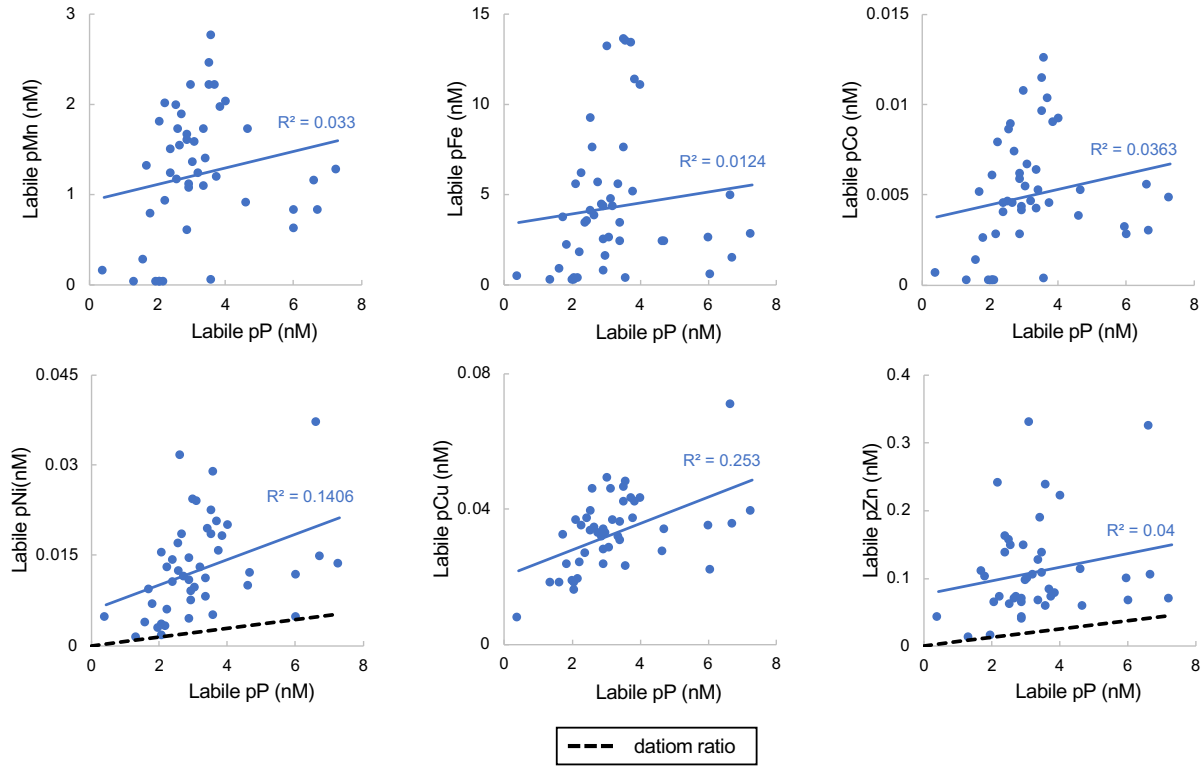

Figure 11. Labile pP (nM) plotted against labile pMn, pFe, pCo, pNi, pCu and pZn for samples >100m depth. Diatom ratios (Twining et al., 2004) are plotted for labile pNi and pZn (black dashed line).

although this comes with additional uncertainties as the community structure is variable and strongly dependent on the interplay of physical conditions (e.g. mixing and irradiance) and macro- and micro-nutrient concentrations (Schofield et al., 2015). For all stations, except the open ocean station located in the marginal sea ice zone (station 53), estimated biogenic pMn contributions are ≤2% below 100m. The ice shelf front inflow (station 42) and outflow (station 36) have low biogenic pMn contributions throughout the water column of respectively ≤2% and ≤1%. The polynya stations (stations 33, 34, 45, 48, 49, and polynya boundary station 52) have estimated contributions of up to 15% in the upper 100m, with highest contributions in the upper 50m. Highest contributions are estimated in the upper 50m of the open ocean station (station 53), with a maximum biogenic contribution of 20%. This station is located off the shelf and is therefore located further from direct lithogenic sources. Particulate concentrations are consequently lower here and when normalized to pP, which is not significantly lower off shelf, yield higher biogenic pMn contributions. Biogenic pFe contributions follow the same trend as pMn, negligible concentrations throughout the water column at the ice shelf front stations (stations 43, 36) and below 100m at the remaining stations. Highest contributions in the upper 100m are similarly found in the polynya stations (stations 33, 34, 45, 48, 49, and boundary station 52), though higher than for pMn, and range between ~10% and ~50%, with one exception of >100% (see explanation below). Biogenic pNi and pZn contributions are overall significantly higher than pMn and pFe biogenic contributions. Highest contributions are similarly found in the upper 100m of the water column and generally range between ~30% and >100%. Below 100m, contributions are lower, but high when compared to pMn and pFe contributions deeper in the water column. Contributions in the deeper waters are not lower than ~10% and generally range between ~10 and ~40%, with exceptions for the open ocean station (station 52) and polynya boundary station (station 52).

It is remarkable that the upper 100m of the water column at most stations has relatively low biogenic pMn and pFe contributions, considering sampling took place during the spring-summer bloom and high phytoplankton biomass was encountered. The remainder of labile pMn and pFe, both in the upper 100m and deeper water column, thus likely consists of abiotic labile particles. This is also demonstrated by the linear regressions with pP (Figure 11), particulate Mn and Fe do not show a significant relationship with pP. It is however possible that there is an underestimation of biogenic pMn and pFe. There could for instance be adsorption of Mn and Fe onto biogenic particles or preferential remineralisation of P relative to Mn and Fe, resulting in higher phytoplankton and detritus Mn/P and Fe/P ratios. Furthermore, detritus is usually enriched with bacterial biomass, which may have higher Fe/P ratios (Tortell et al., 1996). As mentioned before, the diatom ratios used for the calculation could be un-representative for the ASP phytoplankton community and therefore cause an inaccurate estimated biogenic contribution. In contrast to pMn and pFe, pNi and pZn do have significant biogenic contributions. The linear regressions with pP (Figure 11 and Figure 12) demonstrate that pNi and pZn have strong correlations with pP. The pNi and pZn pool are thus mostly dominated by biogenic particles. Over or underestimation is possible however for the same reasons as described above for pMn and pFe. Another point of concern is that for pFe, pNi and pZn several samples have estimated biogenic contribution that exceed 100%. This is not possible in reality and is the result of trace metal/P sample ratios that are lower than the diatom ratios used for the calculation. This indicates that the diatom ratios by Twining et al. (2014) are likely unrepresentative for the true ratios of biogenic material in the ASP.

An additional caveat to the estimation of the biogenic fraction is the fact that not all pP was extracted by the labile leach, as would be expected if all pP were of biogenic origin. Approximately 20% of pP resides in the refractory fraction and 80% in the labile pool. Rauschenberg and Twining (2015) similarly reported that approximately one fifth of pP is present in the refractory pool. This suggests the labile leach is not 100% effective in extracting all labile material or that pP is associated with other (refractory) forms of suspended particulate matter. The latter is unlikely, since the refractory pP distribution (section 4.4.3, Figure 6) closely resembles the labile pP, fluorescence and oxygen distributions (Figure 5, Figure 6). These are indicators for biomass, and not refractory material. There is thus likely a biogenic or detrital fraction that is inaccessible to the labile leach. By calculating the biogenic contribution to the refractory trace metal pool in the same fashion as before, the labile biogenic contributions can be corrected for the amount of trace metals that were supposedly not leached based on refractory particulate P concentrations (Appendix B1 and Appendix B2). The corrected samples are generally not more than 5% higher than the uncorrected samples, with a few exceptions going up to 10%.

To summarize, biogenic pMn and pFe particles are relatively minor components of labile pMn and pFe in the upper 100m of the water column. In the water column below 100m and at the ice shelf front stations, biogenic pMn and pFe contributions are negligibly small. The majority of labile pMn and pFe thus consist of other types of abiotic labile particulate matter. In contrast to pMn and pFe, pNi and pZn are dominated by biogenic particulate matter in the upper 100m. Biogenic pNi and pZn contributions also constitute a significant part of labile pNi and pZn deeper in the water column and at the ice shelf front stations. The trends of the calculated biogenic contributions are supported by the distributions presented in section 4 and the linear regressions with pP (Figure 11 and Figure 12). The labile pNi and pZn distributions closely resemble the labile pP distribution and correlate well, whereas the labile pFe and pMn distributions do not resemble the particulate P distribution and have no significant correlations with pP.

5.2.2 Lithogenic contribution

Lithogenic particulate trace metals are defined as trace metals adsorbed to or incorporated in crustal material and sedimentary particles. This includes trace metals incorporated in or adsorbed to alumino-silicate clay minerals and crystalline oxyhydroxide minerals. The elements Al and Ti both occur in relatively high abundance in the earth's crust and have no key biological functions (De Baar et al., 2017). All pAl and pTi are therefore assumed to be of crustal origin. Similar to the biogenic approach, linear regression of trace metals against pAl and pTi evaluates the potential consistent lithogenic source to the particulate trace metal pool. Since pAl and pTi concentrations had a strong significant correlation (section 4.3.1), linear regression was only performed with pAl for simplification (Figure 12).

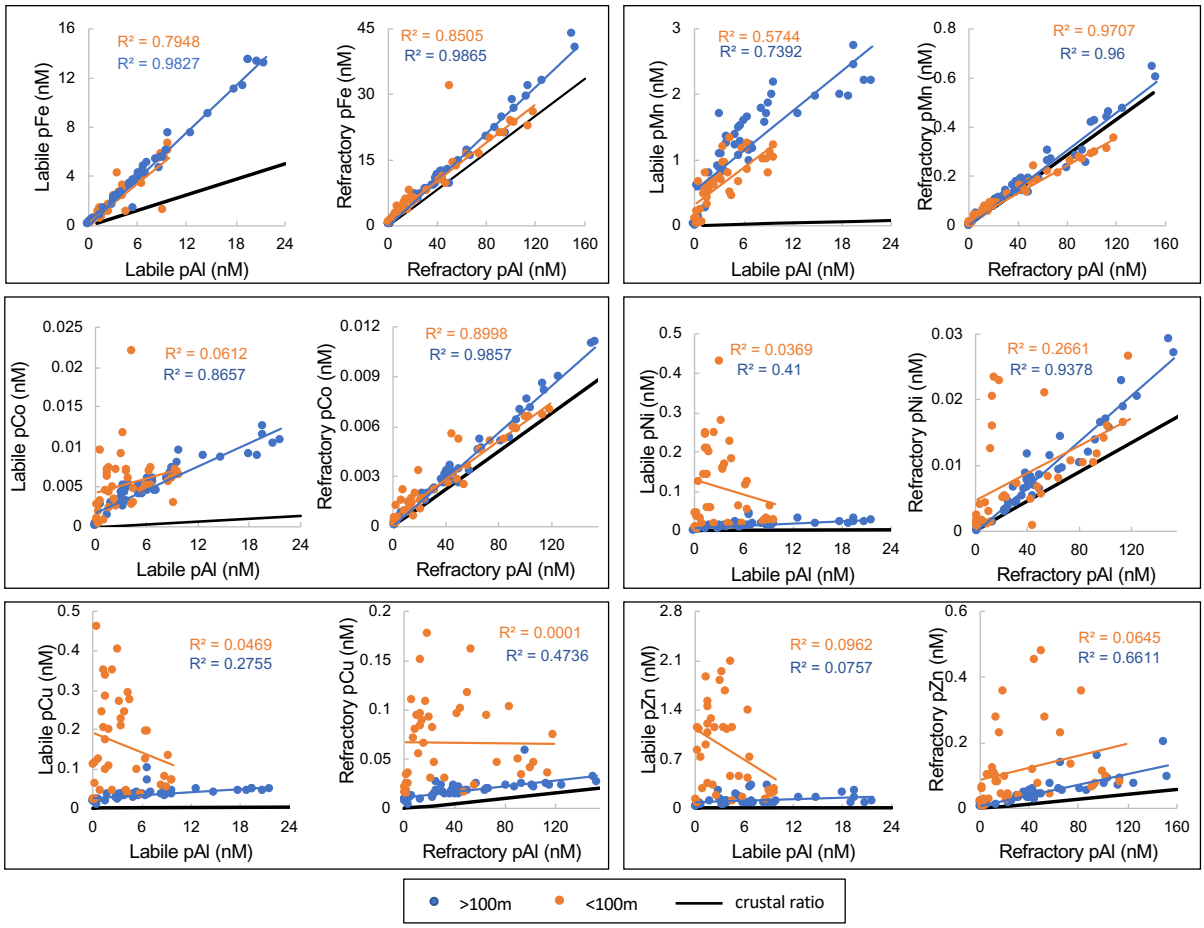

Figure 12. Linear regressions of pFe, pMn, pCo, pNi, pCu and pZn with pAl for both labile and refractory fractions. Samples <100m depth are indicated by orange dots, samples >100m depth are indicated by blue dots. Upper crustal ratios for Fe, Mn, Co, Ni, Cu and Zn are plotted by black lines (Taylor and McLennan, 1985, 1995).

Labile pFe and refractory pFe both have strong correlations with pAl ($p<0.05$) throughout the entire water column. This indicates that both fractions of pFe have a consistent lithogenic source in both the euphotic zone and deeper waters. The estimated biogenic contribution to labile pFe suggests that a significant portion of the labile pFe pool consists of abiotic particles. The significant correlation between labile pFe and pAl in the upper 100m indicates that this, or a portion thereof, could indeed be of lithogenic origin. Similar to pFe, pMn also has significant correlations ($p<0.05$) with pAl throughout the water column, pointing out that there is a consistent lithogenic source to both the labile and refractory pMn pool as well. This again resonates with the estimation that a significant part of labile pMn consist of abiotic particles. Labile pCo has an insignificant relationship with pAl ($p>0.05$) in the upper 100m and a strong significant relationship with particulate Al ($p<0.05$) below 100m. Labile pCo therefore likely has a consistent lithogenic component in the deeper water column, whereas it possibly has a more consistent biogenic component in the upper 100m since labile pCo and pP have a significant correlation in the surface layer. Labile pNi, pCu and pZn in the upper 100m of the water column do not show strong correlations with pAl, corroborating that the fractions likely consist of mostly biogenic particles (section 5.1.1). The refractory fractions do show significant relationships with pAl, indicating that these fractions likely do have a consistent lithogenic component.

Similar to the biogenic approach, assuming all pAl and pTi are of crustal origin, the crustal contribution can be estimated from the crustal trace metal/Al and trace metal/Ti ratios (Planquette et al., 2013). The upper crustal Fe/Al ratio is 0.21 mol mol^{-1}, Fe/Ti ratio is 10 mol mol^{-1}, Mn/Al ratio is 0.0036 mol mol^{-1} and Mn/Ti ratio is 0.17 mol mol^{-1} (Taylor and McLennan, 1985, 1995). Crustal contributions were calculated for pMn and pFe with both Al and Ti crustal ratios, since these elements seem to have consistent lithogenic components throughout the water column for both labile and refractory fractions (Appendix C1 and C2). Based on Al estimated crustal contributions, labile pMn only consists for a very small fraction of crustal material (<7%). The remainder of labile pMn, that is not of biogenic origin, could consist of resuspended sediments and/or authigenic mineral phases such as Mn oxyhydroxide minerals. In contrast, refractory pMn consists almost entirely of crustal particles. Refractory pMn has estimated crustal contributions ranging from ~80% to >100%. Crustal material comprises approximately a third of the labile pFe pool. Approximately a third (taking the biogenic component into account) of the labile pFe pool thus consists of labile abiotic particles that are not of crustal origin. Similar to pMn, these could consist of resuspended sediments or authigenic phases such as Fe oxides and oxyhydroxides. The refractory pFe pool consists of ~50% to >100% of crustal material.

With these calculations the same problem arises as for the calculation of the biogenic fractions, contributions that exceed 100%. Refractory pMn and pFe have several Al ratios that are lower than the crustal ratio resulting in contributions of >100%. The above calculations were performed with Al ratios, but when calculating the crustal contribution with Ti ratios, all refractory crustal Mn contributions and refractory and total Fe contributions exceed >100%. This is similarly caused by sample trace metal/Ti ratios lower than the crustal Ti ratio. It is thus possible that the crustal Al and especially Ti ratios are not representative of the crustal material that is delivered to the ASP. Since most over-estimations were calculated with Ti ratios, there could be an additional source of pMn, pFe and pTi, but little to no pAl that would cause pMn/Ti and pFe/Ti ratios to be significantly lower than the crustal ratio. Reductive dissolution has been observed to supply dissolved Mn and Fe to Antarctic shelf waters (e.g. Sedwick et al., 2011). Elevated dissolved Ti concentrations in euxinic conditions near the ocean floor in the Baltic Sea, compared to non-elevated dissolved Al concentrations, indicate that Ti increases solubility in anoxic/euxinic conditions (Rolison, 2016). Anoxic conditions in bottom sediments of the ASP, possibly due to remineralisation of sinking organic matter from the phytoplankton bloom, or in sediments beneath the ice shelves, could potentially lead to reductive dissolution of Mn, Fe and Ti. If these dissolved species were to precipitate into particles again in the water column, this could lead to sample pFe/Ti and pMn/Ti ratios lower than the crustal ratios if Ti is present in greater amounts than in crustal material. A portion of the pMn and pFe pool would then consist of authigenic minerals that have an indirect lithogenic source. This process can however not be confirmed with the data available in this study.

Planquette et al. (2013) calculated sediment contributions for total pMn based on the sedimentary Mn/Al ratio of 0.011 mol mol^{-1} in the Amundsen Sea (Angino, 1966). They assume that an unsorted resuspension source has a Mn/Al ratio of 0.011 mol mol^{-1}, and that samples with a higher ratio have additional Mn

sources. They do not specify what these sources could be. They also note that there is a small subset of samples with a pMn/Al ratio lower than 0.11 mol mol^{-1}. They assign this as 100% bulk sediment Mn, but mention that crustal contributions would bring the ratio below the sediment ratio. For this study, refractory pMn/Al ratios are significantly lower than the sediment Mn/Al ratio, resulting in refractory sediment contributions of >100% for all samples. Labile pMn/Al ratios are significantly higher than the sediment ratio. For refractory pFe, samples have ratios both lower and higher than the sediment ratio of 0.26 mol mol^{-1} (Angino et al., 1966). Labile pFe/Al ratios are all, except for one sample, higher than both crustal and sediment ratios. It has to be noted that bulk sediment likely consists of a combination of labile and refractory trace metals; e.g. a combination of (weathered) crustal material and authigenic Mn and Fe minerals such as Mn and Fe oxides and oxyhydroxides. Therefore, it makes more sense to look at the total (summed labile and refractory) pMn and pFe fractions. If all samples fell between the crustal and sediment ratio, the relative contributions could be calculated by means of a two-endmember mixing model. Plotting total pMn and pFe against total pAl however shows that for pMn all samples are equal to or higher than the sediment ratio and that for pFe samples both fall between the crustal and sediment ratio and are higher than the sediment ratio (Figure 13). This suggests there are third endmembers which are more enriched in Mn and Fe relative to Al than in sediment. The nature of this potential third end member is unknown. Reductive dissolution and subsequent precipitation in the water column could possibly explain this issue. The ratios of the potentially precipitated particulates by reductive dissolution are, however, not known. Accurately calculating the relative sedimentary and possibly authigenic contributions with the data available in this study is therefore not possible.

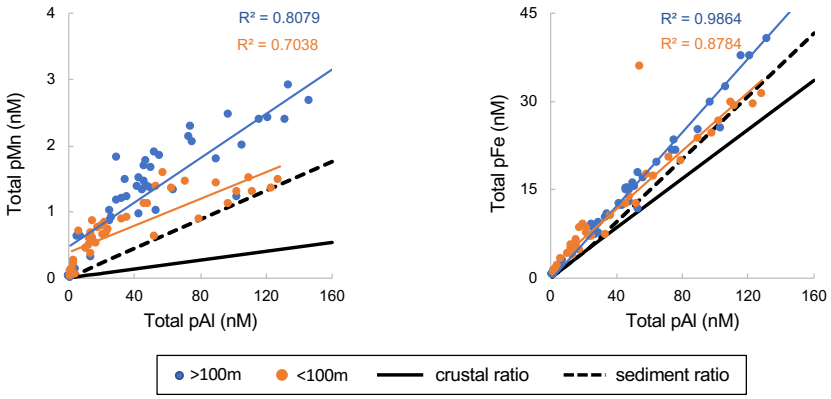

Figure 13. Linear regression of total pMn and total pFe with total pAl. Samples <100m depth are indicated by orange dots, samples >100m depth are indicated by blue dots. Crustal ratios are presented by black lines (Taylor and McLennan, 1985, 1995) and sediment ratios are presented by black dashed lines (Angino, 1966).

In short, refractory fractions of pMn and pFe consist for the majority of crustal material. Labile pMn consists largely of an undefined labile component, likely associated to suspended sediments and authigenic phases such as Mn-oxides or oxyhydroxide minerals. Labile pFe consists for a significant part crustal material, although approximately a third likely also consists of other undefined labile particulate phases that could be associated to suspended sediments or authigenic minerals such as Fe oxyhydroxides. Reductive dissolution and subsequent precipitation in the water column could potentially explain part of the undefined labile phases. However, the data available in this study cannot confirm this.

5.3 Particulate trace metal sources

The phytoplankton blooms as observed in the ASP, can only be sustained by a relatively constant Fe supply throughout the growing season (Alderkamp et al., 2015). The high primary productivity in the ASP (Arrigo and van Dijken 2003, 2015) thus suggests that there are micro-nutrient sources in the ASP that are not available in the open Southern Ocean. There are several potential sources that can deliver particulate trace metals to the ASP. These sources include atmospheric continental dust deposition, melting sea ice, melting glaciers and ice shelves and sediment resuspension. Of these sources, inflow of mCDW in sub-ice shelf cavities, which causes glacial melt and sediment resuspension, is most likely the dominant source for delivery of particulate trace metals to the ASP and thus responsible for the high productivity in the polynya (e.g. Sherrell et al., 2015; Planquette et al., 2013). The potential sources of particulate trace metal delivery and their relative contributions are discussed below.

5.3.1 Atmospheric dust deposition

There are no known direct dust inputs in the proximity of the Amundsen Sea (Gerringa et al., 2012). The open Southern Ocean receives aeolian dust from continental sources in Australia, South Africa and Argentina. Cassar et al. (2007) showed that net community production correlates with input of aeolian dust to the Southern Ocean. The dust supply to the Southern Ocean is low however (Jickells et al., 2005). Gerringa et al. (2012) calculated that atmospheric dust input contributes to less than 0.1% of dissolved Fe required to sustain the phytoplankton blooms in the Amundsen Sea. Planquette et al. (2013) similarly concluded that continental dust input can only account for a very small fraction of pFe delivered to the water column of the Amundsen Sea. They calculated that the dust flux in the Southern Ocean would yield a steady state pFe concentration of 0.11-31 pM in the upper 10m of the water column, much lower than pFe concentrations found in their study. In the context of this study, the supposed steady state dust Fe concentration is at least ~35 times lower than total pFe concentrations in the upper 10m at open ocean station (station 53), which is located off the shelf and is thus most comparable to open Southern Ocean conditions. The steady state concentration is at least ~300 to ~1000 times lower than pFe concentrations in the upper 10m of the polynya and ice shelf front stations. Direct aeolian dust input to the water column can thus only be responsible for a tiny fraction of total particulate trace metals in the upper water column, especially in the polynya. Dust input is therefore likely an insignificant source in supplying trace metals to the phytoplankton bloom compared to other sources. Indirect sources of aeolian dust, such as dust deposited on sea ice, ice shelves or glaciers do not belong to this fraction and might provide a higher, although indirect, source.

5.3.2 Sea ice melt

Particulate trace metals can be incorporated in sea ice via mechanisms such as sediment resuspension at time of sea ice formation, atmospheric dust deposition or inclusion of biogenic particles in sea ice. Upon melt of the sea ice the particulate trace metals are released into the upper water column and can potentially support primary productivity. Studies have showed that pFe can be an important source of bioavailable Fe to phytoplankton in sea ice covered regions (Lannuzel et al., 2014, 2016; Kanna et al., 2020). In the open ocean station (station 53), polynya boundary station (station 52) and the adjacent station located in the central polynya body (station 49) reduced salinities were observed in the upper 10m (section 4.3.1). The low salinity layer was most pronounced at the open ocean station (station 53), which was located in the marginal sea ice zone. The other two stations located in the polynya likely had lower surface salinity layers due to advection of sea ice melt water into these areas since they had been ice-free for some weeks. The only station directly subjected to sea ice melt was thus the open ocean marginal sea ice station (station 53).

Lannuzel et al. (2011) and Van der Merwe et al. (2011) reported on dissolved and particulate trace metal concentrations in east Antarctic fast ice, pack ice and water 1m below the sea ice. They report molar ratios of 0.33 for Fe/Al and 0.006 for Mn/Al in the lower sections of fast ice and argue that these ratios are consistent with the crustal abundance ratios for Fe and Mn according to Taylor and McLennan (1985) and that sediment resuspension is thus dominant in supplying particulates to fast ice. The pFe/Al and Mn/Al ratios in the upper 10m of the marginal sea ice station are respectively 0.48 mol mol^{-1} and 0.06 mol mol^{-1}. These ratios are higher than the upper crustal ratios of 0.21 mol mol^{-1} and 0.0035 mol mol^{-1} for Fe/Al and Mn/Al respectively (Taylor and McLennan, 1985, 1995). The open ocean marginal sea ice station

(station 53) is however not located in a fast ice zone, but in a pack ice zone in the open ocean. Lannuzel et al. (2011) and Van der Merwe et al. (2011) observed higher ratios in pack ice with 0.62 mol mol^{-1} for Fe/Al and 0.011 mol mol^{-1} for Mn/Al. The higher ratios in pack ice compared to fast ice could be caused by adsorption or biological uptake of Fe and Mn, causing pack ice ratios to be higher. The ratios calculated for the upper 10m of the marginal sea ice station (station 53) of this study fall between the fast and pack ice ratios found by Lannuzel et al. (2011) and Van der Merwe et al. (2011). They are thus slightly enriched in Fe and Mn compared to fast ice, but have a more pronounced lithogenic source than true pack ice. Planquette et al. (2013) reported molar ratios for pFe/Al and Mn/Al in low salinity surface layers close to the upper crustal ratios and concluded that this is consistent with a possible sea ice pFe and pMn source. The stations considered were however located on the shelf in the Pine Island section of the Amundsen Sea, rather than off the shelf like the open ocean station (station 53) of this study. This could explain the ratios close to the crustal ratios, since sediment incorporation might play a more important role in sea ice on than off the shelf. The ratios in the upper 10m of the open ocean marginal sea ice station of this study, are thus more enriched in Fe and Mn than the ratios found by Planquette et al. (2013) and fall between the fast and pack ice ratios found by Lannuzel et al. (2011) and Van der Merwe et al. (2011) and therefore seem to be more enriched with lithogenic material than particulate ratios in true pack ice. The Mn/Al and Fe/Al ratios in the upper 10m of the open ocean marginal sea ice station indicate that a sea ice source to these particles is possible. It has to be noted, however, that upon melt the particulate trace metals are released into the water column where they mix with the pre-existing particulate trace metal pool. The ratios therefore do not necessarily indicate a sea ice source of the particulate matter.

Sherrell et al. (2015) reported on dissolved trace metal dynamics in the ASP and concluded that sea ice melt may periodically be a source of dissolved Fe to the upper water column, but that this is limited to the early bloom stage which consumes all sea ice released dissolved Fe. They also argue that surface maxima of dissolved Fe at low salinity surface waters were not observed for any other trace metals, implying that these maxima are not caused by sea ice melt since this would also yield maxima for other trace metals (Lannuzel et al., 2011). At the open ocean marginal sea ice station (station 53) no pronounced surface maxima in the upper 10m were present for any of the analysed particulate trace metals in this study. This suggests that sea ice melt is not the primary source of particulate trace metals in the upper 10m of the open ocean station (station 53). If a sea ice melt signature is indeed present in particulate trace metal pool, it is at least overwhelmed by other sources of greater magnitude who likely contribute more to sustaining the phytoplankton bloom.

Sea ice melt does however play an important role in bloom development by enhancing stratification and thereby creating increased light availability (Sherrell et al., 2015; Schofield et al, 2015). Alderkamp et al. (2015) found that highest productivity was located where sea ice melt signatures showed enhanced stratification combined with increased light availability. Furthermore, autonomous glider observations found a correlation between phytoplankton biomass and enhanced stratification (Schofield et al., 2015). A decreased mixed layer depth as a result of stratification by sea ice melt thus increases irradiance in the upper water column allowing dense phytoplankton blooms to form. The enhanced stratification due to sea ice melt is indeed observed at the marginal sea ice station and outmost stations in the polynya (stations 53, 52 and 49). This indicates that even in late bloom conditions at the end of January sea ice melt plays a role in sustaining the phytoplankton bloom by increasing stratification and thus irradiance, rather than supplying bioavailable particulate trace metals.

5.3.3 Glacial meltwater and sediment resuspension

Outflow of glacial meltwater beneath ice shelves in the Amundsen Sea has been suggested to be the main source of trace metals, in particular Fe, that fuels the phytoplankton blooms in these regions (e.g. Gerringa et al., 2012, Sherrell et al., 2015; Planquette et al., 2013). Intrusion of mCDW onto the shelf and into the sub-ice cavities of the DIS causes melting on the underside of the floating ice shelf and at the base of the grounded glacier. In this way, sediment or crustal particles entrained in the ice shelf or glacial ice are transported to the ASP with the outflow of mCDW underneath the ice shelves. The in- and outflow of mCDW also entrains suspended sediments from underneath the ice shelves, adding these to the particulate trace metals that are present in the outflow. No studies have assessed the direct content of particulate trace metals in the DIS outflow and the labile, and therefore potentially bioavailable, fraction of these particles.

The results of this study show that pAl and pTi are highly enriched in both labile and refractory fractions at the ice shelf front outflow stations (stations 34 and 36). At these same stations, pFe, pMn and pCo have similar trends. Refractory pNi and pZn are also present in elevated concentrations at the outflow stations. The highest concentrations of these elements in the entire transect are found at the DIS outflow stations (stations 34 and 36), implying that DIS outflow is indeed the primary source of these trace metals to the ASP. Sherrell et al. (2015) sampled one station at the DIS front, located near the outflow station of this study (station 36). Measurements of current velocities at the station showed a strong northward outflow and the water had a high fraction of glacial meltwater (1.5%), indicating the station was indeed located in the DIS outflow. The apparent outflow was enriched in dissolved Fe, dissolved Cu and suspended particulate matter. The concentrations of dissolved Fe in the upper 300m were similar to concentrations measured by Gerringa et al. (2012), confirming that the outflow of Fe enriched mCDW is a permanent characteristic. Enriched pFe concentrations were similarly found in the DIS outflow in this study. However, enriched pCu was not observed in the outflow. Sherrell et al. (2015) furthermore observed that the outflow was only slightly enriched in dissolved Mn. They argue that coastal sedimentary input or input from bottom sediments may be of greater magnitude than the DIS outflow for dissolved Mn. The large plumes of labile and refractory pMn observed in this study were thus not represented in the dissolved phase studied by Sherrell et al. (2015). The pMn enriched outflow water could thus potentially be the major source of bioavailable Mn to the polynya. Sherrell et al. (2015) similarly observed no to little enrichment of dissolved Ni and Zn in the outflow. They suggest that most of the dissolved Ni and Zn present on the shelf was delivered by inflow of mCDW, since concentrations did not vary much from open ocean concentrations. This study however showed that the outflow is enriched in refractory pNi and pZn. Since the labile distributions of pZn and pNi do not have elevated concentrations in the outflow (section 4.4.3), the bioavailable Zn and Ni needed for the phytoplankton bloom could indeed come from ACC waters off shelf as suggested by Sherrell et al. (2015).

Planquette et al. (2013) found pFe/Al and pMn/Al ratios at ice shelf stations that were respectively near the crustal and sediment ratios. This suggest that pFe and pMn at these stations consisted mostly of crustal material derived from the ice shelves and glaciers and from resuspended sediments beneath the ice shelves or at the base of the glaciers. Total pFe/Al ratios at the ice shelf outflow stations of this study are slightly higher than the upper crustal ratio and total crustal contributions were approximately 60% to 80%. This suggests that the outflow is enriched in pFe by mostly crustal material, although enhanced by sedimentary and possibly authigenic inputs. Total pMn/Al ratios at these stations were significantly higher than the upper crustal ratio and rather approached the bulk sediment ratio of 0.011 mol mol^{-1} (Agino, 1966). Crustal pMn contributions were therefore not more than 30% at the outflow stations. This suggest the outflow is enriched in pMn by mostly suspended sediments and possibly other authigenic particulates (as potentially formed by reductive dissolution and subsequent precipitation).

The particulate trace metal distributions of this study show that a significant portion of pFe, pMn and pCo delivered by DIS outflow are labile, suggesting that the DIS outflow provides the ASP with large amounts of trace metals that are potentially bioavailable or can become bioavailable in a matter of days (Berger et al., 2008). The labile pMn and pFe in the DIS outflow plume have negligible biogenic contributions and small crustal contributions, implying that the remainder of labile material consists of other labile abiotic particles, for example derived from resuspended sediments, oxyhydroxide minerals or other authigenic minerals. Alderkamp et al. (2015) concluded based on incubation experiments that dissolved Fe

concentrations do not seem to be a good indicator of Fe availability for phytoplankton in the ASP and that pFe is or becomes part of the bioavailable trace metal pool. They suggest that crustal particles or Fe oxyhydroxides may be made bioavailable by processes such as dissolution or photo reduction. It is thus very likely, that the labile pFe and pMn supplied by the DIS outflow are transported to the euphotic zone by processes such as mixing and advective transport, and once arrived, are made bio-available to the phytoplankton community. The DIS outflow thus likely fuels the phytoplankton bloom by not only providing dissolved trace metals, but also providing a large flux of labile and thus potentially bioavailable trace metals to the ASP.

Besides elevated concentrations at the DIS outflow, concentrations were also elevated throughout the water column at the central polynya station 48. The elevated concentrations are present for the same elements that have enriched concentrations at the DIS outflow; pMn, pFe, pCo, refractory pNi and refractory pZn. The higher concentrations could be caused by either sediment resuspension or DIS outflow water. The maximum concentrations are located at the deepest sample at station 48, near the bottom of the water column. Since station 48 is located on the eastern flank of the Dotson Trough, in theory inflow of CDW is expected here, and not outflow. Though a meandering outflow or specific outflow branch is possible. Moreover, the DIS outflow is less dense than mCDW inflow due to mixing with meltwater, so the maximum concentrations would not be expected at the lowermost samples near the sea floor. This suggests the enhanced concentrations could be caused by sediment resuspension. Additionally, the oxygen concentration at the lowermost sample of station 48 is 4.47 ml L^{-1}. Oxygen concentrations as measured by an autonomous glider in the central through were less than 4.5 ml L^{-1}, consistent with values of mCDW, and between 5 and 5.5 ml L^{-1} in the DIS outflow (Miles et al., 2016). Solely based on oxygen concentrations, the water present at station 48 is inflow of mCDW. This would mean the elevated concentrations could be caused by sediment resuspension. However, oxygen concentrations can also be locally lowered at this location as a result of remineralisation of organic matter that sank down from the euphotic zone, as the station is located in the central polynya where primary productivity is high. Ratios of pMn/Al and pFe/Al similarly do not give an answer to the question, as Mn/Al and Fe/Al ratios at station 48 are similar to pMn/Al and pFe/Al ratios in the DIS outflow for both labile and refractory fractions. Based on the data available in this study it is not possible to distinguish between sediment resuspension or DIS outflow at this location in the transect.

5.4 The future of the ASP

This study shows that the DIS outflow is the main source of labile particulate bio-essential trace metals to the ASP. Increased melt rates could thus cause an increased flux of these trace metals to the ASP. Alderkamp et al. (2015) performed incubation experiments in the build-up phase of the phytoplankton bloom in the ASP and showed that dissolved Fe addition significantly increases photosynthesis rates, which are already high compared to other polynyas (Arrigo and van Dijken, 2003, 2015). They conclude that Fe availability may limit phytoplankton growth rates in areas of the ASP. Antarctic ice sheets in the Amundsen Sea embayment are experiencing rapid thinning, upstream glaciers are retreating and accelerating in flow and basal melt is increasing (e.g. Rignot et al., 2013, 2014; Mouginot et al., 2014). Increased basal melt and subsequent increased DIS outflow would most likely be caused by an increase in heat content of mCDW flowing underneath the DIS (e.g. Jacobs et al., 2011). Alderkamp et al. (2015) argue that increased outflow could destabilize the water column near the ice shelf front, causing an increase of mixed layer depth and thereby decreasing light availability to phytoplankton near the ice shelf. This scenario could have an effect in the early season when irradiance is still low. The bloom commencement could potentially be delayed resulting in lower productivity. They also note that if the DIS is a source of bioavailable Fe to the ASP, an increase in DIS outflow which is transported to the surface layer of the central polynya that was stratified by sea ice melt could cause increased primary productivity. Increased DIS outflow with its associated particulate trace metal concentrations could thus further enhance the magnitude of the phytoplankton bloom in the ASP if the particulate metals, notably pFe and pMn, are bioavailable.

A recent study by Park et al. (2017) investigated the interplay between Fe effects and light availability in the ASP and PIP. Bio-physical analysis showed that phytoplankton were Fe limited in the ASP, as also suggested by Alderkamp et al. (2015), whereas Fe conditions were still replete in the PIP during late austral summer. Park et al (2017) suggest that light availability rather than Fe controlled the magnitude of the phytoplankton bloom in the PIP. The ASP was subjected to a higher solar irradiance and showed a higher chlorophyll biomass than the PIP. Park et al. (2017) argue that due to expanding ice-free areas, mixing could increase in the future due to stronger winds, which in turn could cause reduction in light availability by expansion of the mixed layer. Additionally, phytoplankton in low light conditions generally have a higher Fe requirement and some phytoplankton species can deal better with low light conditions than other species. There could thus be an additional community composition effect as result of changing light conditions. Implications for the ASP could be the following; if trace metal supply increases due to an increase in meltwater and DIS outflow, this could lead to an initial increase in productivity until the threshold of light limitation is reached, e.g. by self-shading of the phytoplankton community or light limitations by expansion of the mixed layer depth due to increasing winds as argued by Park et al. (2017). The question remains on what time scale light availability in the ASP would become limiting compared to increased trace metal inputs and if this point will be reached at all.

6. Conclusion

This study analysed the particulate trace metal dynamics in the ASP along a transect that follows the in - and outflow path of mCDW through the Dotson Trough. The particulate trace metal samples were analysed for labile and refractory fractions to assess the potential bioavailability of the particulate suspended matter present in the water column. The particulate trace metal distributions could generally be grouped according to two types of distributions; the first type having elevated concentrations at the DIS outflow stations (pMn, pFe, pCo, refractory pNi, refractory pZn) and the second type having highest concentrations in the upper 100m of the water column (labile pNi, pCu, labile pZn), with exception of stations located at the DIS front. The distributions with elevated concentrations at the DIS outflow stations generally correlated strongly with the non-biological pAl and pTi, which are assumed to be of lithogenic origin. The distributions with highest concentrations in the upper 100m of the water column generally correlated strongly with pP, which is assumed to be of biogenic origin.

Regressions of the bio-essential trace metals with pP shows that pMn and pFe do not have a consistent biogenic component in both the upper 100m of the water column and deeper waters. Calculation of the relative biogenic contribution confirms this, a significant fraction of labile pMn and pFe consist of undefined abiotic labile particles. Labile pCo, pNi, pCu and pZn do have consistent biogenic sources as they correlate significantly with pP. Calculation of the relative biogenic contribution of labile pNi and pZn supports this and shows that they primarily consist of biogenic material in the upper water column. To assess the lithogenic component, regressions of the bio-essential elements with pAl were performed. This illustrated that pMn, pFe and refractory pCo have consistent lithogenic components and labile pCo, pNi, pCu and pZn do not have a consistent lithogenic component. Calculation of the relative crustal component shows that refractory pMn and pFe for the majority consist of crustal material. Labile pMn and pFe only partly consist of crustal material, and thus likely consist of sediments and authigenic minerals for the significant remaining part.

The results show that direct atmospheric dust deposition is a negligible source compared to other trace metal sources in the ASP. Sea ice melt is similarly a minor source of particulate trace metals. Both sources are likely present, but are overwhelmed by the particulate trace metal inputs of other sources. Glacial melt and sediment resuspension by in- and outflow of mCDW beneath the DIS is the major source of pMn, pFe, pCo, refractory pNi and refractory pZn. This is the first study to shows that the DIS outflow is the main supplier of particulate trace metals, more specifically, labile particulate trace metals to the ASP. The phytoplankton community can potentially benefit from this input on a short time scale, since labile particulate material can be made bioavailable in a matter of days. This implies that particulate trace metals present in the DIS outflow likely partly fuel the phytoplankton bloom in the ASP. Increased input of particulate trace metals due to increased glacial melt and ice sheet thinning in the future could thus lead to increased primary productivity and the consequent enhanced uptake of atmospheric CO_2, and thereby potentially provide a small negative feedback to climate change.

Future research could focus on the interplay between increased trace metal input and light limitation and on what timescales, and if at all, light limitation could play a role in the ASP. Bioassay experiments or modelling studies could provide potential insights into this matter. The relative contribution of particulate versus dissolved trace metals to sustaining the phytoplankton bloom and how the flux of these different phases could change in the future is another point for further research. Furthermore, the relative input of particulate and dissolved trace metals by the different ice shelves bordering the Amundsen Sea has to be quantified to a greater extent to allow for more accurate estimations of fluxes of trace metals into the ASP and how these might change in the future.

References

Alderkamp, A. C., Mills, M. M., van Dijken, G. L., Laan, P., Thuróczy, C. E., Gerringa, L. J. A., … Arrigo, K. R. (2012). Iron from melting glaciers fuels phytoplankton blooms in the Amundsen Sea (Southern Ocean): Phytoplankton characteristics and productivity. *Deep-Sea Research Part II: Topical Studies in Oceanography*, *71–76*, 32–48. https://doi.org/10.1016/j.dsr2.2012.03.005

Alderkamp, A. C., Van Dijken, G. L., Lowry, K. E., Connelly, T. L., Lagerström, M., Sherrell, R. M., … Arrigo, K. R. (2015). Fe availability drives phytoplankton photosynthesis rates during spring bloom in the Amundsen Sea Polynya, Antarctica. *Elementa*, *3*(C), 1–26. https://doi.org/10.12952/journal.elementa.000043

Angino, E. E. (1966). Geochemistry of Antarctic pelagic sediments. *Geochimica et Cosmochimica Acta*, *30*(9), 939-961.

Arrigo, K. R., & van Dijken, G. L. (2003). Phytoplankton dynamics within 37 Antarctic coastal polynya systems. *Journal of Geophysical Research C: Oceans*, *108*(8), 27–1. https://doi.org/10.1029/2002jc001739

Arrigo, K. R., van Dijken, G. L., & Bushinsky, S. (2008). Primary production in the Southern Ocean, 1997-2006. *Journal of Geophysical Research: Oceans*, *113*(8), 1997–2006. https://doi.org/10.1029/2007JC004551

Arrigo, K. R., van Dijken, G., & Long, M. (2008). Coastal Southern Ocean: A strong anthropogenic CO2 sink. *Geophysical Research Letters*, *35*(21), 1–6. https://doi.org/10.1029/2008GL035624

Arrigo, K. R., Lowry, K. E., & van Dijken, G. L. (2012). Annual changes in sea ice and phytoplankton in polynyas of the Amundsen Sea, Antarctica. *Deep Sea Research Part II: Topical Studies in Oceanography*, *71*, 5-15.

Arrigo, K. R., van Dijken, G. L., & Strong, A. L. (2015). Environmental controls of marine productivity hot spots around A ntarctica. *Journal of Geophysical Research: Oceans*, *120*(8), 5545-5565.

Berger, C. J., Lippiatt, S. M., Lawrence, M. G., & Bruland, K. W. (2008). Application of a chemical leach technique for estimating labile particulate aluminum, iron, and manganese in the Columbia River plume and coastal waters off Oregon and Washington. *Journal of Geophysical Research: Oceans*, *113*(C2).

Chester, R., & Hughes, M. J. (1967). A chemical technique for the separation of ferro-manganese minerals, carbonate minerals and adsorbed trace elements from pelagic sediments. *Chemical geology*, *2*, 249-262.

Cullen, J. T., & Sherrell, R. M. (1999). Techniques for determination of trace metals in small samples of size-fractionated particulate matter: phytoplankton metals off central California. *Marine Chemistry*, *67*(3-4), 233-247.

De Baar, H. J., de Jong, J. T., Bakker, D. C., Löscher, B. M., Veth, C., Bathmann, U., & Smetacek, V. (1995). Importance of iron for plankton blooms and carbon dioxide drawdown in the Southern Ocean. *Nature*, *373*(6513), 412-415.

De Baar, H. J., Timmermans, K. R., Laan, P., De Porto, H. H., Ober, S., Blom, J. J., … & Klunder, M. (2008). Titan: A new facility for ultraclean sampling of trace elements and isotopes in the deep oceans in the international Geotraces program. *Marine Chemistry*, *111*(1-2), 4-21.

De Baar, H. J. W., van Heuven, S. M. A. C., & Middag, R. (2017). Ocean biochemical cycling and trace elements. *Encyclopedia of Earth Sciences Series*.

Frölicher, T. L., Sarmiento, J. L., Paynter, D. J., Dunne, J. P., Krasting, J. P., & Winton, M. (2015). Dominance of the Southern Ocean in anthropogenic carbon and heat uptake in CMIP5 models. *Journal of Climate*, *28*(2), 862–886. https://doi.org/10.1175/JCLI-D-14-00117.1

Gerringa, L. J. A., Alderkamp, A. C., Laan, P., Thuróczy, C. E., De Baar, H. J. W., Mills, M. M., … Arrigo, K. R. (2012). Iron from melting glaciers fuels the phytoplankton blooms in Amundsen Sea (Southern Ocean): Iron biogeochemistry. *Deep-Sea Research Part II: Topical Studies in Oceanography*, *71–76*, 16–31. https://doi.org/10.1016/j.dsr2.2012.03.007

Goldberg, E. D. (1954). Marine geochemistry 1. Chemical scavengers of the sea. The Journal of Geology, 62(3), 249-265.

Hurst, M. P., Aguilar-Islas, A. M., & Bruland, K. W. (2010). Iron in the southeastern Bering Sea: Elevated leachable particulate Fe in shelf bottom waters as an important source for surface waters. *Continental Shelf Research*, *30*(5), 467–480. https://doi.org/10.1016/j.csr.2010.01.001

Jacobs, S. S., Jenkins, A., Giulivi, C. F., & Dutrieux, P. (2011). Stronger ocean circulation and increased melting under Pine Island Glacier ice shelf. *Nature Geoscience*, *4*(8), 519–523. https://doi.org/10.1038/ngeo1188

Jenkins, A., Dutrieux, P., Jacobs, S. S., McPhail, S. D., Perrett, J. R., Webb, A. T., & White, D. (2010). Observations beneath Pine Island Glacier in West-Antarctica and implications for its retreat. *Nature Geoscience*, *3*(7), 468–472. https://doi.org/10.1038/ngeo890

Jensen, L. T., Wyatt, N. J., Landing, W. M., & Fitzsimmons, J. N. (2020). Assessment of the stability, sorption, and exchangeability of marine dissolved and colloidal metals. Marine Chemistry, 103754.

Kanna, N., Lannuzel, D., van der Merwe, P., & Nishioka, J. (2020). Size fractionation and bioavailability of iron released from melting sea ice in a subpolar marginal sea. *Marine Chemistry*, *221*, 103774.

Khatiwala, S., Primeau, F., & Hall, T. (2009). Reconstruction of the history of anthropogenic CO2 concentrations in the ocean. *Nature*, *462*(7271), 346–349. https://doi.org/10.1038/nature08526

Landschützer, P., Gruber, N., Haumann, F. A., Rödenbeck, C., Bakker, D. C. E., Heuven, S. Van, … Takahashi, T. (2015). Ocean carbon sink. *Science*, *349*(6253), 1221–1224. https://doi.org/10.1126/science.aab2620

Lannuzel, D., Bowie, A. R., van der Merwe, P. C., Townsend, A. T., & Schoemann, V. (2011). Distribution of dissolved and particulate metals in Antarctic sea ice. *Marine Chemistry*, *124*(1-4), 134-146.

Lannuzel, D., van der Merwe, P. C., Townsend, A. T., & Bowie, A. R. (2014). Size fractionation of iron, manganese and aluminium in Antarctic fast ice reveals a lithogenic origin and low iron solubility. *Marine Chemistry*, *161*, 47-56.

Lannuzel, D., Chever, F., van der Merwe, P. C., Janssens, J., Roukaerts, A., Cavagna, A. J., … & Meiners, K. M. (2016). Iron biogeochemistry in Antarctic pack ice during SIPEX-2. *Deep Sea Research Part II: Topical Studies in Oceanography*, *131*, 111-122.

Martin, J. H., Gordon, R. M., & Fitzwater, S. E. (1990). Iron in Antarctic waters. *Nature*, *345*(6271), 156-158.

Martin, J. H., Fitzwater, S. E., & Gordon, R. M. (1990). Iron deficiency limits phytoplankton growth in Antarctic waters. *Global Biogeochemical Cycles*, *4*(1), 5-12.

Mikaloff Fletcher, S. E., Gruber, N., Jacobson, A. R., Doney, S. C., Dutkiewicz, S., Gerber, M., ... Sarmiento, J. L. (2006). Inverse estimates of anthropogenic CO2 uptake, transport, and storage by the ocean. *Global Biogeochemical Cycles*, *20*(2), 1–16. https://doi.org/10.1029/2005GB002530

Mitchell, B. G., & Holm-Hansen, O. (1991). Observations of modeling of the Antartic phytoplankton crop in relation to mixing depth. *Deep Sea Research Part A. Oceanographic Research Papers*, *38*(8-9), 981-1007.

Monteiro, T., Kerr, R., Orselli, I. B. M., & Lencina-Avila, J. M. (2020). Towards an intensified summer CO2 sink behaviour in the Southern Ocean coastal regions. *Progress in Oceanography*, 102267. https://doi.org/10.1016/j.pocean.2020.102267

Mouginot, J., Rignot, E., & Scheuchl, B. (2014). Sustained increase in ice discharge from the Amundsen Sea Embayment, West Antarctica, from 1973 to 2013. *Geophysical Research Letters*, *41*(5), 1576-1584.

Nitsche, F. O., Jacobs, S. S., Larter, R. D., & Gohl, K. (2007). Bathymetry of the Amundsen Sea continental shelf: Implications for geology, oceanography, and glaciology. *Geochemistry, Geophysics, Geosystems*, *8*(10).

Park, J., Kuzminov, F. I., Bailleul, B., Yang, E. J., Lee, S., Falkowski, P. G., & Gorbunov, M. Y. (2017). Light availability rather than Fe controls the magnitude of massive phytoplankton bloom in the Amundsen Sea polynyas, Antarctica. *Limnology and Oceanography*, *62*(5), 2260-2276.

Planquette, H., & Sherrell, R. M. (2012). Sampling for particulate trace element determination using water sampling bottles: methodology and comparison to in situ pumps. *Limnology and Oceanography: Methods*, *10*(5), 367-388.

Planquette, H., fy, R. M., Stammerjohn, S., & Field, M. P. (2013). Particulate iron delivery to the water column of the Amundsen Sea, Antarctica. *Marine Chemistry*, *153*, 15–30. https://doi.org/10.1016/j.marchem.2013.04.006

Ohnemus, D. C., Auro, M. E., Sherrell, R. M., Lagerström, M., Morton, P. L., Twining, B. S., ... & Lam, P. J. (2014). Laboratory intercomparison of marine particulate digestions including Piranha: a novel chemical method for dissolution of polyethersulfone filters. *Limnology and Oceanography: Methods*, *12*(8), 530-547.

Rauschenberg, S., & Twining, B. S. (2015). Evaluation of approaches to estimate biogenic particulate trace metals in the ocean. *Marine Chemistry*, *171*, 67-77.

Rignot, E., Bamber, J. L., Van Den Broeke, M. R., Davis, C., Li, Y., Van De Berg, W. J., & Van Meijgaard, E. (2008). Recent Antarctic ice mass loss from radar interferometry and regional climate modelling. *Nature Geoscience*, *1*(2), 106–110. https://doi.org/10.1038/ngeo102

Rignot, E., Jacobs, S., Mouginot, J., & Scheuchl, B. (2013). Ice-shelf melting around Antarctica. *Science*, *341*(6143), 266-270.

Rignot, E., Mouginot, J., Morlighem, M., Seroussi, H., & Scheuchl, B. (2014). Widespread, rapid grounding line retreat of Pine Island, Thwaites, Smith, and Kohler glaciers, West Antarctica, from 1992 to 2011. *Geophysical Research Letters*, *41*(10), 3502-3509

Rijkenberg, M. J., de Baar, H. J., Bakker, K., Gerringa, L. J., Keijzer, E., Laan, M., ... & Ossebaar, S. (2015). "PRISTINE", a new high volume sampler for ultraclean sampling of trace metals and isotopes. *Marine Chemistry*, *177*, 501-509.

Rolison, J. (2016). *The biogeochemistry of trace metals and their isotopes in the Mediterranean and Black Seas* (Doctoral dissertation, University of Otago).

Sabine, C. L., Feely, R. A., Gruber, N., Key, R. M., Lee, K., Bullister, J. L., ... & Millero, F. J. (2004). The oceanic sink for anthropogenic CO2. *Science*, *305*(5682), 367-371.

Sarmiento, J. L., Gruber, N., Brzezinski, M. A., & Dunne, J. P. (2004). High-latitude controls of thermocline nutrients and low latitude biological productivity. *Nature*, *427*(6969), 56–60. https://doi.org/10.1038/nature02127

Schlitzer, R. (2020) Ocean Data View, https://odv.awi.de

Sherrell, R. M., Lagerström, M. E., Forsch, K. O., Stammerjohn, S. E., & Yager, P. L. (2015). Dynamics of dissolved iron and other bioactive trace metals (Mn, Ni, Cu, Zn) in the Amundsen Sea Polynya, Antarctica. *Elementa*, *3*, 1–27. https://doi.org/10.12952/journal.elementa.000071

Sigman, D. M., & Boyle, E. A. (2000). Glacial/Interglacial changes in atmospheric carbon dioxide. *Nature*, *407*(October), 859–869.

Smith, W. O., & Comiso, J. C. (2008). Influence of sea ice on primary production in the Southern Ocean: A satellite perspective. *Journal of Geophysical Research: Oceans*, *113*(5), 1–19. https://doi.org/10.1029/2007JC004251

St-Laurent, P., Yager, P. L., Sherrell, R. M., Oliver, H., Dinniman, M. S., & Stammerjohn, S. E. (2019). Modeling the Seasonal Cycle of Iron and Carbon Fluxes in the Amundsen Sea Polynya, Antarctica. *Journal of Geophysical Research: Oceans*, *124*(3), 1544–1565. https://doi.org/10.1029/2018JC014773

St-Laurent, P., Yager, P. L., Sherrell, R. M., Stammerjohn, S. E., & Dinniman, M. S. (2017). Pathways and supply of dissolved iron in the Amundsen Sea (Antarctica). *Journal of Geophysical Research: Oceans*, *122*(9), 7135–7162. https://doi.org/10.1002/2017JC013162

Sunda, W. G. (1989). Trace metal interactions with marine phytoplankton. Biological Oceanography, 6(5-6), 411-442.

Sunda, W. G., & Huntsman, S. A. (1997). Interrelated influence of iron, light and cell size on marine phytoplankton growth. *Nature*, *390*(6658), 389-392.

Taylor, S. R., & McLennan, S. M. (1985). The continental crust: its composition and evolution.

Taylor, S. R., & McLennan, S. M. (1995). The geochemical evolution of the continental crust. *Reviews of geophysics*, *33*(2), 241-265.

Turekian, K. K., & KK, T. (1977). The fate of metals in the oceans.

Twining, B. S., Baines, S. B., & Fisher, N. S. (2004). Element stoichiometries of individual plankton cells collected during the Southern Ocean Iron Experiment (SOFeX). *Limnology and oceanography*, *49*(6), 2115-2128.

Twining, B. S., & Baines, S. B. (2013). The trace metal composition of marine phytoplankton. *Annual review of marine science*, *5*, 191-215.

Van der Merwe, P., Lannuzel, D., Bowie, A. R., Nichols, C. M., & Meiners, K. M. (2011). Iron fractionation in pack and fast ice in East Antarctica: Temporal decoupling between the release of dissolved and particulate iron during spring melt. *Deep Sea Research Part II: Topical Studies in Oceanography*, *58*(9-10), 1222-1236.

Walker, D. P., Brandon, M. A., Jenkins, A., Allen, J. T., Dowdeswell, J. A., & Evans, J. (2007). Oceanic heat transport onto the Amundsen Sea shelf through a submarine glacial trough. *Geophysical Research Letters*, *34*(2).

Yager, P. L., Sherrell, R. M., Stammerjohn, S. E., Alderkamp, A. C., Schofield, O., Abrahamsen, E. P., ... Wilson, S. (2012). ASPIRE: The Amundsen sea Polynya international research expedition. *Oceanography*, *25*(3), 40–53. https://doi.org/10.5670/oceanog.2012.73

Appendix A Acid, filter and process blanks

Acid, filter and process blanks averages ± 1SD in units of pmol/vial for the labile leach (labile), subsequent total digestion (refractory) and separate total digestion (total). All blanks were corrected for outliers by omitting values that did not fall within ± 2SD of the blank average.

	Al	P	Ti	V	Mn	Fe	Co	Ni	Cu	Zn	Cd	Pb
Acid blank												
Labile	288.88	55.91	1.02	2.04	0.99	42.69	0.22	13.09	3.60	128.10	0.100	0.157
± 1SD	210.40	26.77	0.51	1.06	0.53	26.42	0.09	6.24	2.67	171.75	0.111	0.148
Acid blank												
Refractory	205.46	174.70	25.99	1.58	0.34	15.93	0.29	7.91	1.42	34.43	0.072	1.639
± 1SD	33.30	213.91	7.19	0.63	0.19	9.42	0.17	2.09	0.46	40.00	0.049	1.996
Acid blank												
Total	206.54	73.38	33.75	2.21	0.25	9.17	0.23	7.90	11.94	22.28	0.042	0.062
± 1SD	12.83	9.77	10.35	0.07	0.05	2.30	0.22	0.34	21.40	18.68	0.009	0.060
Filter blank												
Labile	358.56	93.34	2.88	0.68	1.39	42.48	0.27	15.86	3.64	223.07	0.136	0.443
± 1SD	145.98	80.97	2.52	0.08	0.26	9.63	0.08	6.99	2.02	83.94	0.042	0.141
Filter blank												
Refractory	302.70	74.12	188.32	0.86	0.68	33.06	0.44	10.81	2.91	37.91	0.057	0.820
± 1SD	111.29	19.34	44.10	0.11	0.22	9.00	0.33	3.18	1.21	24.43	0.052	1.053
Process blank												
Labile	1389.56	3765.14	26.25	5.24	76.53	897.32	1.13	232.46	81.07	417.92	1.045	2.289
± 1SD	635.12	1425.37	14.73	1.06	50.17	462.01	0.07	209.52	31.34	190.73	0.494	0.975
Process blank												
Refractory	5434.07	1818.40	636.35	4.94	18.81	1815.97	0.57	14.98	23.41	65.87	0.075	0.262
± 1SD	3675.70	609.47	260.03	3.14	14.63	1123.07	0.41	10.82	8.13	5.00	0.016	0.184

Appendix B1 Biogenic particulate Mn and Fe contributions

Biogenic contributions of particulate Mn and Fe calculated by Southern Ocean diatom metal quotas of 0.28 mmol Mn/mol P and 1.93 mmol Fe/mol P (Twining et al., 2004). Labile biogenic contributions exceeding 100% are highlighted in bold font.

Station	Depth [m]	labile Mn/P [mmol mol^{-1}]	% biogenic labile Mn	% biogenic labile Mn refractory corrected	total Mn/P [mmol mol^{-1}]	% biogenic total Mn	labile Fe/P [mmol mol^{-1}]	% biogenic labile Fe	% biogenic labile Fe refractory corrected	total Fe/P [mmol mol^{-1}]	% biogenic total Fe
33	768	309.78	0%	0%	265.43	0%	1330.16	0%	0%	3152.81	0%
	690	448.62	0%	0%	359.91	0%	1543.89	0%	0%	4030.31	0%
	592	562.86	0%	0%	406.38	0%	1361.39	0%	0%	3652.63	0%
	443	540.52	0%	0%	417.45	0%	1444.56	0%	0%	3631.02	0%
	195	498.80	0%	0%	403.73	0%	1607.15	0%	0%	3814.95	0%
	146	375.55	0%	0%	287.36	0%	1291.78	0%	0%	3115.74	0%
	97	47.70	1%	1%	44.93	1%	145.86	1%	2%	516.17	0%
	72	3.22	9%	10%	3.07	9%	3.88	50%	53%	20.94	9%
	44	3.07	9%	10%	2.91	10%	2.52	77%	79%	18.97	10%
	19	3.10	9%	10%	2.94	10%	11.18	17%	20%	33.25	6%
	10	3.10	9%	10%	2.93	10%	7.16	27%	30%	30.99	6%
34	542	686.83	0%	0%	528.17	0%	3791.13	0%	0%	8218.23	0%
	492	754.28	0%	0%	526.99	0%	3705.08	0%	0%	8913.64	0%
	393	763.34	0%	0%	539.12	0%	3526.43	0%	0%	8469.65	0%
	295	493.15	0%	0%	409.05	0%	2710.51	0%	0%	6358.18	0%
	186	170.08	0%	0%	141.46	0%	722.64	0%	0%	2095.73	0%
	156	135.21	0%	0%	112.77	0%	419.93	0%	1%	1452.26	0%
	97	11.47	2%	3%	11.40	2%	35.78	5%	7%	189.23	1%
	72	6.17	5%	6%	5.95	5%	14.92	13%	15%	65.95	3%
	48	6.47	4%	5%	6.20	5%	15.81	12%	15%	71.22	3%
	20	6.13	5%	5%	5.89	5%	17.39	11%	13%	72.96	3%
	9	7.59	4%	4%	7.15	4%	26.31	7%	9%	185.20	1%
36	295	717.31	0%	0%	548.35	0%	4292.26	0%	0%	10545.51	0%
	245	584.91	0%	0%	457.80	0%	3551.50	0%	0%	7940.48	0%
	196	500.29	0%	0%	367.87	0%	2895.98	0%	0%	6268.37	0%
	146	21.08	1%	2%	22.11	1%	92.73	2%	2%	458.85	0%
	72	32.60	1%	1%	33.61	1%	190.53	1%	1%	760.87	0%
	32	48.81	1%	1%	49.94	1%	245.28	1%	1%	992.52	0%
	9	46.73	1%	1%	46.67	1%	243.05	1%	1%	960.49	0%
42	769	831.82	0%	0%	604.21	0%	2547.07	0%	0%	6360.35	0%
	690	502.11	0%	0%	376.29	0%	1381.87	0%	0%	3400.49	0%
	641	672.01	0%	0%	505.45	0%	2013.35	0%	0%	5164.90	0%
	542	860.57	0%	0%	588.54	0%	2631.80	0%	0%	6001.31	0%
	344	399.11	0%	0%	310.35	0%	963.06	0%	0%	2547.66	0%
	245	190.52	0%	0%	153.74	0%	501.14	0%	1%	1763.31	0%
	97	41.19	1%	1%	43.76	1%	242.11	1%	1%	871.34	0%
	72	48.13	1%	1%	51.21	1%	305.76	1%	1%	1115.81	0%
	47	21.57	1%	2%	23.23	1%	105.53	2%	2%	494.27	0%

Station	Depth [m]	labile Mn/P [mmol mol^{-1}]	% biogenic labile Mn	% biogenic labile Mn refractory corrected	total Mn/P [mmol mol^{-1}]	% biogenic total Mn	labile Fe/P [mmol mol^{-1}]	% biogenic labile Fe	% biogenic labile Fe refractory corrected	total Fe/P [mmol mol^{-1}]	% biogenic total Fe
42	18	11.37	2%	3%	12.68	2%	60.86	3%	4%	288.88	1%
	11	12.31	2%	3%	13.66	2%	50.91	4%	4%	301.02	1%
45	507	606.19	0%	0%	454.26	0%	1379.70	0%	0%	4244.92	0%
	442	404.43	0%	0%	325.31	0%	1147.86	0%	0%	3238.27	0%
	394	734.37	0%	0%	501.86	0%	2083.75	0%	0%	5277.79	0%
	345	296.14	0%	0%	248.25	0%	867.52	0%	0%	2797.89	0%
	235	370.59	0%	0%	294.43	0%	814.93	0%	0%	2559.97	0%
	176	314.69	0%	0%	241.14	0%	663.05	0%	0%	2088.56	0%
	97	54.94	1%	1%	48.75	1%	153.15	1%	2%	490.27	0%
	73	6.83	4%	5%	6.70	4%	17.26	11%	13%	69.81	3%
	47	3.12	9%	10%	2.94	10%	8.73	22%	25%	30.02	6%
	15	2.61	11%	12%	2.40	12%	6.31	31%	34%	20.68	9%
	10	3.08	9%	11%	2.95	9%	7.74	25%	28%	34.13	6%
48	592	643.83	0%	0%	435.45	0%	2833.67	0%	0%	7032.88	0%
	444	615.91	0%	0%	448.30	0%	2108.26	0%	0%	5390.52	0%
	231	561.72	0%	0%	428.18	0%	1496.28	0%	0%	3987.45	0%
	96	144.41	0%	0%	120.52	0%	471.23	0%	1%	1532.00	0%
	47	12.55	2%	3%	12.25	2%	40.51	5%	6%	171.03	1%
	10	2.70	10%	12%	2.55	11%	4.32	45%	49%	29.69	7%
49	572	496.22	0%	0%	358.78	0%	1474.32	0%	0%	4966.54	0%
	494	359.14	0%	0%	291.71	0%	484.98	0%	1%	1519.79	0%
	443	435.08	0%	0%	329.44	0%	799.96	0%	0%	2417.68	0%
	314	353.79	0%	0%	256.95	0%	491.94	0%	1%	1721.97	0%
	216	171.02	0%	0%	134.60	0%	367.29	1%	1%	1257.70	0%
	156	120.04	0%	0%	95.43	0%	213.86	1%	1%	790.15	0%
	97	55.68	1%	1%	45.39	1%	89.29	2%	3%	374.08	1%
	69	14.89	2%	2%	13.17	2%	25.01	8%	10%	126.13	2%
	38	2.58	11%	13%	2.36	12%	6.52	30%	34%	20.46	9%
	21	2.09	13%	16%	1.90	15%	5.09	38%	42%	21.40	9%
	10	2.18	13%	15%	1.96	14%	4.39	44%	49%	17.88	11%
52	483	159.41	0%	0%	134.48	0%	505.74	0%	1%	2156.42	0%
	394	399.50	0%	0%	290.81	0%	737.29	0%	0%	2605.02	0%
	295	200.66	0%	0%	160.07	0%	214.33	1%	1%	754.94	0%
	146	100.35	0%	0%	76.94	0%	80.82	2%	3%	287.56	1%
	97	22.50	1%	2%	19.38	1%	37.21	5%	6%	121.72	2%
	57	10.46	3%	3%	8.78	3%	22.33	9%	11%	66.42	3%
	25	2.22	13%	14%	2.03	14%	4.39	44%	48%	13.12	15%
	9	2.04	14%	16%	1.79	16%	1.80	**107%**	**106%**	8.15	24%
53	1015	12.04	2%	3%	11.33	2%	122.81	2%	2%	303.71	1%
	789	6.57	4%	5%	6.41	4%	102.05	2%	2%	202.63	1%
	690	6.83	4%	5%	6.50	4%	92.36	2%	3%	186.94	1%
	542	8.12	3%	5%	7.40	4%	114.40	2%	2%	234.60	1%
	394	5.67	5%	6%	5.69	5%	88.82	2%	3%	198.81	1%

Station	Depth [m]	labile Mn/P [mmol mol^{-1}]	% biogenic labile Mn	% biogenic labile Mn refractory corrected	total Mn/P [mmol mol^{-1}]	% biogenic total Mn	labile Fe/P [mmol mol^{-1}]	% biogenic labile Fe	% biogenic labile Fe refractory corrected	total Fe/P [mmol mol^{-1}]	% biogenic total Fe
53	196	9.52	3%	4%	8.44	3%	71.32	3%	3%	174.22	1%
	97	4.61	6%	8%	4.19	7%	46.48	4%	5%	105.57	2%
	67	2.19	13%	16%	2.13	13%	30.45	6%	8%	70.57	3%
	37	1.43	20%	23%	1.28	22%	7.68	25%	29%	18.46	10%
	24	1.49	19%	22%	1.30	22%	3.85	50%	55%	13.31	14%
	10	1.77	16%	19%	1.55	18%	4.42	44%	49%	13.53	14%

Appendix B2 Biogenic particulate Ni and Zn contributions

Biogenic contributions of particulate Ni and Zn calculated by Southern Ocean diatom metal quotas of 0.73 mmol Ni/mol P and 6.2 mmol Zn/mol P (Twining et al., 2004). Labile and total biogenic contributions exceeding 100% are highlighted in bold font. Refractory corrected labile biogenic contributions calculated from refractory biogenic contributions exceeding 100% are similarly highlighted in bold font.

Station	Depth [m]	labile Ni/P [mmol mol^{-1}]	% biogenic labile Ni	% biogenic labile Mn refractory corrected	total Ni/P [mmol mol^{-1}]	% biogenic total Ni	labile Zn/P [mmol mol^{-1}]	% biogenic labile Zn	% biogenic labile Zn refractory corrected	total Zn/P [mmol mol^{-1}]	% biogenic total Zn
33	768	4.11	18%	23%	4.69	16%	18.68	33%	40%	25.43	24%
	690	4.70	16%	21%	5.64	13%	23.27	27%	34%	24.86	25%
	592	6.76	11%	16%	7.27	10%	24.90	25%	34%	29.05	21%
	443	4.88	15%	20%	5.31	14%	23.29	27%	34%	25.71	24%
	195	3.19	23%	29%	3.99	18%	19.01	33%	40%	22.04	28%
	146	3.91	19%	25%	4.22	17%	32.10	19%	26%	28.09	22%
	97	1.10	66%	71%	1.25	58%	26.15	24%	28%	23.03	27%
	72	1.07	68%	**71%**	1.00	73%	7.86	79%	**81%**	7.32	85%
	44	0.96	76%	**78%**	0.89	82%	7.26	85%	**87%**	6.59	94%
	19	1.25	58%	**62%**	1.15	63%	8.76	71%	**74%**	7.76	80%
	10	1.15	64%	**67%**	1.08	68%	7.25	85%	87%	7.52	82%
34	542	6.25	12%	17%	7.45	10%	37.85	16%	23%	40.69	15%
	492	7.96	9%	15%	9.05	8%	64.85	10%	16%	68.16	9%
	393	6.55	11%	18%	7.67	10%	60.26	10%	16%	51.39	12%
	295	4.88	15%	20%	5.97	12%	54.11	11%	16%	52.56	12%
	186	5.57	13%	17%	5.18	14%	48.65	13%	17%	42.76	14%
	156	1.91	38%	46%	2.29	32%	16.23	38%	46%	15.12	41%
	97	1.15	63%	**68%**	1.01	72%	13.71	45%	51%	13.94	44%
	72	1.03	71%	**75%**	0.92	80%	9.60	65%	**69%**	8.87	70%
	48	1.06	69%	**73%**	0.90	81%	11.35	55%	**59%**	9.94	62%
	20	1.07	68%	**72%**	0.88	83%	7.17	87%	89%	8.28	75%
	9	0.99	73%	**77%**	0.84	87%	7.15	87%	89%	8.33	74%
36	295	7.88	9%	15%	10.07	7%	31.21	20%	29%	36.81	17%
	245	5.44	13%	19%	6.99	10%	21.78	28%	38%	26.82	23%
	196	4.61	16%	24%	6.31	12%	19.59	32%	44%	21.95	28%
	146	0.92	80%	82%	1.06	69%	6.35	98%	98%	8.13	76%
	72	0.96	76%	80%	1.18	62%	8.04	77%	81%	8.85	70%
	32	1.10	67%	71%	1.38	53%	8.45	73%	77%	10.69	58%
	9	0.92	79%	83%	1.16	63%	5.87	**106%**	104%	7.26	85%
42	769	7.11	10%	15%	7.33	10%	29.38	21%	30%	34.66	18%
	690	4.25	17%	24%	4.24	17%	66.42	9%	13%	56.90	11%
	641	4.07	18%	25%	4.92	15%	25.90	24%	32%	30.89	20%
	542	5.63	13%	20%	7.04	10%	31.12	20%	30%	54.15	11%
	344	5.53	13%	18%	5.20	14%	54.41	11%	15%	46.80	13%
	245	2.10	35%	43%	2.42	30%	23.96	26%	33%	22.60	27%
	97	0.96	76%	79%	1.27	58%	7.16	87%	89%	10.88	57%
	72	1.27	58%	62%	1.66	44%	12.48	50%	55%	13.09	47%
	47	1.16	63%	68%	1.37	53%	NA	NA	NA	NA	NA

Station	Depth [m]	labile Ni/P [mmol mol^{-1}]	% biogenic labile Ni	% biogenic labile Ni refractory corrected	total Ni/P [mmol mol^{-1}]	% biogenic total Ni	labile Zn/P [mmol mol^{-1}]	% biogenic labile Zn	% biogenic labile Zn refractory corrected	total Zn/P [mmol mol^{-1}]	% biogenic total Zn
42	18	1.06	69%	72%	1.05	69%	7.71	80%	83%	8.40	74%
	11	0.77	95%	96%	0.77	95%	5.99	**104%**	**103%**	5.82	**107%**
45	507	5.74	13%	18%	5.69	13%	54.86	11%	16%	48.08	13%
	442	3.57	20%	27%	3.61	20%	53.25	12%	16%	48.05	13%
	394	5.15	14%	22%	5.42	13%	61.54	10%	16%	49.90	12%
	345	10.73	7%	NA	7.55	10%	97.77	6%	8%	85.78	7%
	235	2.44	30%	37%	2.82	26%	14.17	44%	52%	17.54	35%
	176	2.35	31%	39%	2.98	25%	36.75	17%	23%	31.27	20%
	97	1.68	43%	49%	1.68	43%	16.00	39%	45%	14.33	43%
	73	1.22	60%	**64%**	1.05	69%	7.50	83%	85%	8.27	75%
	47	1.78	41%	**45%**	1.58	46%	7.53	82%	85%	7.58	82%
	15	1.16	63%	**67%**	1.00	73%	5.03	**123%**	**119%**	4.76	**130%**
	10	1.10	66%		0.90	81%	6.27	99%	**99%**	5.70	**109%**
48	592	11.89	6%	10%	9.86	7%	56.00	11%	18%	46.97	13%
	444	5.12	14%	21%	5.47	13%	29.86	21%	29%	28.24	22%
	231	3.68	20%	27%	4.47	16%	21.67	29%	37%	23.99	26%
	96	2.32	31%	39%	2.39	31%	16.81	37%	45%	15.61	40%
	47	1.24	59%	**63%**	1.10	66%	7.15	87%	89%	7.86	79%
	10	0.95	77%		0.79	92%	4.41	**141%**	**132%**	3.81	**163%**
49	572	7.49	10%	15%	6.80	11%	104.23	6%	9%	76.80	8%
	494	2.54	29%	35%	2.65	28%	12.15	51%	58%	12.87	48%
	443	3.09	24%	31%	3.07	24%	31.34	20%	26%	29.48	21%
	314	3.01	24%	33%	2.70	27%	49.25	13%	18%	35.72	17%
	216	1.86	39%	48%	1.83	40%	9.26	67%	74%	9.16	68%
	156	2.16	34%	42%	1.95	38%	15.40	40%	49%	13.24	47%
	97	1.80	40%	48%	1.58	46%	12.87	48%	56%	11.53	54%
	69	1.32	55%	**61%**	1.12	65%	7.15	87%	**89%**	6.09	**102%**
	38	0.77	94%	NA	0.63	**115%**	4.82	**129%**	**122%**	4.96	**125%**
	21	0.83	88%	**89%**	0.71	**103%**	5.29	**117%**	**114%**	4.50	**138%**
	10	0.75	97%	**98%**	0.61	**119%**	7.55	82%	**85%**	6.57	94%
52	483	2.26	32%	40%	2.14	34%					
	394	2.53	29%	38%	2.59	28%	106.12	6%	9%	77.72	8%
	295	1.49	49%	56%	1.45	50%	13.13	47%	55%	12.57	49%
	146	0.77	95%	**96%**	0.71	**103%**	10.91	57%	**64%**	9.26	67%
	97	0.59	**125%**	**119%**	0.51	**143%**	7.13	87%	**89%**	6.12	**101%**
	57	0.57	**129%**	**121%**	0.49	**150%**	11.97	52%	**58%**	10.14	61%
	25	0.30	NA	NA	0.25	**296%**	6.59	94%	**95%**	5.83	**106%**
	9	0.37	**196%**	**168%**	0.31	**234%**	8.62	72%	**76%**	7.39	84%
53	1015	0.90	82%	NA	0.64	**115%**	7.33	85%	88%	8.99	69%
	789	1.36	54%	**59%**	1.09	67%	NA	NA	NA	NA	NA
	690	0.71	NA	NA	0.43	**171%**	NA	NA	NA	NA	NA
	542	1.53	48%	65%	1.19	62%	NA	NA	NA	NA	NA
	394	1.40	52%	NA	1.02	72%	7.25	86%	88%	14.58	43%
	196	1.33	55%	61%	1.23	59%	15.71	39%	46%	14.48	43%

Station	Depth [m]	labile Ni/P [mmol mol^{-1}]	% biogenic labile Ni	% biogenic labile Mn refractory corrected	total Ni/P [mmol mol^{-1}]	% biogenic total Ni	labile Zn/P [mmol mol^{-1}]	% biogenic labile Zn	% biogenic labile Zn refractory corrected	total Zn/P [mmol mol^{-1}]	% biogenic total Zn
53	97	0.88	83%	**86%**	0.80	91%	10.88	57%	**63%**	8.98	69%
	67	0.72	**101%**	**101%**	0.69	**106%**	11.12	56%	**62%**	9.40	66%
	37	0.64	**114%**	**111%**	0.53	**137%**	14.42	43%	**48%**	12.37	50%
	24	0.65	**113%**	**110%**	0.55	**133%**	16.47	38%	**43%**	13.68	45%
	10	0.70	**104%**	**103%**	0.59	**125%**	17.95	35%	**40%**	15.06	41%

Appendix C1 Crustal particulate Mn contributions

Crustal contributions of particulate Mn calculated with crustal ratios of 0.0036 mol Mn/mol Al and 0.17 mol Mn/mol Ti. Crustal contributions exceeding 100% are highlighted in bold font.

Station	Depth [m]	labile Mn/Al [mol mol^{-1}]	labile Mn/Ti [mol mol^{-1}]	% crustal labile Mn Al	% crustal labile Mn Ti	refractory Mn/Al [mol mol^{-1}]	refractory Mn/Ti [mol mol^{-1}]	% crustal refractory Mn Al	% crustal refractory Mn Ti	total Mn/Al [mol mol^{-1}]	total Mn/Ti [mol mol^{-1}]	% crustal total Mn Al	% crustal total Mn Ti
33	768	0.162	8.272	2%	2%	0.004	0.091	85%	**186%**	0.027	0.640	13%	27%
	690	0.185	12.736	2%	1%	0.004	0.087	82%	**196%**	0.029	0.634	12%	27%
	592	0.259	21.662	1%	1%	0.004	0.076	95%	**223%**	0.036	0.800	10%	21%
	443	0.256	11.699	1%	1%	0.004	0.088	89%	**192%**	0.037	0.872	10%	19%
	195	0.189	9.402	2%	2%	0.004	0.096	84%	**178%**	0.036	0.876	10%	19%
	146	0.173	10.578	2%	2%	0.004	0.081	89%	**210%**	0.029	0.644	12%	26%
	97	0.181	24.753	2%	1%	0.004	0.086	91%	**199%**	0.025	0.604	14%	28%
	72	0.372	111.224	1%	0%	0.004	0.064	83%	**267%**	0.047	0.774	8%	22%
	44	0.540	135.560	1%	0%	0.005	0.068	75%	**250%**	0.056	0.860	6%	20%
	19	0.204	21.827	2%	1%	0.005	0.052	66%	**328%**	0.042	0.488	8%	35%
	10	0.263	62.305	1%	0%	0.005	0.049	77%	**344%**	0.039	0.478	9%	36%
34	542	0.125	5.587	3%	3%	0.004	0.089	90%	**190%**	0.022	0.519	17%	33%
	492	0.139	9.798	3%	2%	0.004	0.099	83%	**171%**	0.020	0.496	18%	34%
	393	0.133	7.308	3%	2%	0.004	0.094	87%	**182%**	0.021	0.503	17%	34%
	295	0.111	4.992	3%	3%	0.004	0.094	88%	**181%**	0.020	0.494	18%	34%
	186	0.165	11.893	2%	1%	0.003	0.067	**111%**	**252%**	0.020	0.459	18%	37%
	156	0.213	18.236	2%	1%	0.003	0.080	**106%**	**213%**	0.022	0.546	17%	31%
	97	0.178	23.253	2%	1%	0.003	0.077	**114%**	**222%**	0.016	0.405	23%	42%
	72	0.303	30.780	1%	1%	0.005	0.080	79%	**211%**	0.027	0.516	13%	33%
	48	0.254	21.317	1%	1%	0.004	0.083	95%	**205%**	0.024	0.559	15%	30%
	20	0.241	20.705	1%	1%	0.004	0.059	101%	**290%**	0.023	0.405	16%	42%
	9	0.329	49.081	1%	0%	0.004	0.087	101%	**196%**	0.026	0.663	14%	26%
36	295	0.101	5.957	4%	3%	0.004	0.089	91%	**192%**	0.016	0.391	22%	44%
	245	0.106	5.290	3%	3%	0.004	0.087	95%	**195%**	0.018	0.456	20%	37%
	196	0.103	5.538	4%	3%	0.004	0.081	93%	**209%**	0.018	0.418	20%	41%
	146	0.144	22.042	3%	1%	0.003	0.066	**136%**	**258%**	0.012	0.314	30%	54%
	72	0.111	15.429	3%	1%	0.003	0.071	**125%**	**238%**	0.012	0.307	31%	55%
	32	0.123	11.956	3%	1%	0.003	0.070	**125%**	**241%**	0.014	0.357	26%	48%
	9	0.119	12.381	3%	1%	0.003	0.072	**127%**	**236%**	0.013	0.341	29%	50%
42	769	0.211	13.392	2%	1%	0.004	0.092	91%	**184%**	0.027	0.679	13%	25%
	690	0.236	12.376	2%	1%	0.004	0.102	81%	**167%**	0.033	0.814	11%	21%
	641	0.204	9.972	2%	2%	0.004	0.096	89%	**178%**	0.029	0.729	12%	23%
	542	0.205	10.244	2%	2%	0.005	0.102	77%	**166%**	0.031	0.717	12%	24%
	344	0.269	14.989	1%	1%	0.004	0.078	**101%**	**217%**	0.035	0.830	10%	20%
	245	0.274	25.834	1%	1%	0.003	0.079	**131%**	**215%**	0.019	0.577	19%	29%
	97	0.109	9.035	3%	2%	0.003	0.074	**126%**	**228%**	0.012	0.334	30%	51%
	72	0.107	7.957	3%	2%	0.003	0.071	**131%**	**239%**	0.011	0.299	33%	57%
	47	0.118	15.937	3%	1%	0.003	0.077	**122%**	**221%**	0.011	0.318	31%	53%

Station	Depth [m]	labile Mn/Al [mol mol^{-1}]	labile Mn/Ti [mol mol^{-1}]	% crustal labile Mn Al	% crustal labile Mn Ti	refractory Mn/Al [mol mol^{-1}]	refractory Mn/Ti [mol mol^{-1}]	% crustal refractory Mn Al	% crustal refractory Mn Ti	total Mn/Al [mol mol^{-1}]	total Mn/Ti [mol mol^{-1}]	% crustal total Mn Al	% crustal total Mn Ti
42	18	0.119	13.177	3%	1%	0.003	0.066	**125%**	**258%**	0.011	0.266	33%	64%
	11	0.127	19.603	3%	1%	0.003	0.076	**120%**	**224%**	0.011	0.305	32%	56%
45	507	0.265	19.953	1%	1%	0.004	0.095	91%	**178%**	0.033	0.848	11%	20%
	442	0.230	11.183	2%	2%	0.005	0.101	78%	**168%**	0.033	0.782	11%	22%
	394	0.226	10.770	2%	2%	0.004	0.090	85%	**189%**	0.031	0.718	11%	24%
	345	0.212	6.308	2%	3%	0.003	0.048	**106%**	**356%**	0.032	0.480	11%	35%
	235	0.316	15.712	1%	1%	0.004	0.088	96%	**192%**	0.034	0.849	10%	20%
	176	0.339	23.344	1%	1%	0.004	0.016	92%	**1062%**	0.036	0.162	10%	**105%**
	97	0.233	21.710	2%	1%	0.004	0.072	100%	**236%**	0.029	0.632	12%	27%
	73	0.193	26.695	2%	1%	0.004	0.084	84%	**202%**	0.027	0.593	13%	29%
	47	0.234	69.517	2%	0%	0.005	0.041	77%	**410%**	0.038	0.388	10%	44%
	15	0.343	41.384	1%	0%	0.004	0.041	89%	**415%**	0.047	0.535	8%	32%
	10	0.370	32.821	1%	1%	0.004	0.057	92%	**297%**	0.030	0.473	12%	36%
48	592	0.134	7.810	3%	2%	0.003	0.084	**111%**	**202%**	0.019	0.525	19%	32%
	444	0.222	9.933	2%	2%	0.003	0.085	**111%**	**199%**	0.025	0.694	14%	24%
	231	0.246	13.816	1%	1%	0.004	0.089	93%	**192%**	0.033	0.811	11%	21%
	96	0.196	19.292	2%	1%	0.003	0.088	**110%**	**193%**	0.022	0.630	17%	27%
	47	0.186	17.236	2%	1%	0.003	0.073	**109%**	**234%**	0.020	0.480	18%	35%
	10	0.275	15.196	1%	1%	0.005	0.055	71%	**307%**	0.039	0.470	9%	36%
49	572	0.178	17.016	2%	1%	0.003	0.076	**124%**	**224%**	0.020	0.566	18%	30%
	494	0.510	39.936	1%	0%	0.004	0.098	81%	**173%**	0.062	1.485	6%	11%
	443	0.338	18.643	1%	1%	0.004	0.103	81%	**165%**	0.042	1.051	8%	16%
	314	0.187	36.578	2%	0%	0.004	0.101	84%	**169%**	0.040	1.126	9%	15%
	216	0.310	23.935	1%	1%	0.003	0.084	**113%**	**202%**	0.029	0.805	13%	21%
	156	0.415	45.190	1%	0%	0.004	0.089	100%	**192%**	0.033	0.871	11%	20%
	97	0.086	58.219	4%	0%	0.004	0.078	96%	**217%**	0.027	0.759	14%	22%
	69	0.292	65.205	1%	0%	0.004	0.080	90%	**212%**	0.030	0.651	12%	26%
	38	0.350	29.193	1%	1%	0.003	0.039	**108%**	**432%**	0.030	0.382	12%	44%
	21	0.096	36.047	4%	0%	0.005	0.028	68%	**610%**	0.038	0.308	9%	55%
	10	0.249	15.028	1%	1%	0.005	0.030	76%	**569%**	0.042	0.308	9%	55%
52	483	0.163	11.795	2%	1%	0.004	0.077	98%	**222%**	0.021	0.478	17%	36%
	394	0.300	26.600	1%	1%	0.005	0.090	79%	**190%**	0.040	0.858	9%	20%
	295	0.761	58.270	0%	0%	0.007	0.097	52%	**176%**	0.085	1.295	4%	13%
	146	1.078	127.473	0%	0%	0.005	0.074	73%	**230%**	0.103	1.688	3%	10%
	97	0.528	58.123	1%	0%	0.004	0.055	82%	**309%**	0.061	0.851	6%	20%
	57	0.459	48.548	1%	0%	0.005	0.047	80%	**364%**	0.053	0.612	7%	28%
	25	0.301	31.741	1%	1%	0.006	0.034	61%	**501%**	0.072	0.527	5%	32%
	9	0.991	70.040	0%	0%	0.007	0.054	53%	**313%**	0.106	0.931	3%	18%
53	1015	0.121	10.222	3%	2%	0.004	0.019	87%	**913%**	0.019	0.098	19%	**174%**
	789	0.079	7.722	5%	2%	0.003	0.014	**108%**	**1226%**	0.015	0.075	23%	**225%**
	690	0.096	7.518	4%	2%	0.004	0.021	99%	**797%**	0.017	0.118	21%	**144%**
	542	0.088	8.519	4%	2%	0.002	0.016	**153%**	**1072%**	0.011	0.079	34%	**214%**
	394	0.067	7.324	5%	2%	0.003	0.016	**109%**	**1066%**	0.013	0.074	27%	**229%**

Station	Depth [m]	labile Mn/Al [mol mol^{-1}]	labile Mn/Ti [mol mol^{-1}]	% crustal labile Mn Al	% crustal labile Mn Ti	refractory Mn/Al [mol mol^{-1}]	refractory Mn/Ti [mol mol^{-1}]	% crustal refractory Mn Al	% crustal refractory Mn Ti	total Mn/Al [mol mol^{-1}]	total Mn/Ti [mol mol^{-1}]	% crustal total Mn Al	% crustal total Mn Ti
53	196	0.117	19.976	3%	1%	0.003	0.027	**128%**	**638%**	0.018	0.196	20%	87%
	97	0.076	19.219	5%	1%	0.004	0.016	86%	**1037%**	0.022	0.114	16%	**150%**
	67	0.050	14.837	7%	1%	0.004	0.023	97%	**749%**	0.014	0.112	25%	**151%**
	37	0.204	26.516	2%	1%	0.004	0.027	84%	**623%**	0.035	0.266	10%	64%
	24	0.189	34.544	2%	0%	0.005	0.017	74%	**1008%**	0.057	0.274	6%	62%
	10	0.350	46.714	1%	0%	0.006	0.040	58%	**420%**	0.056	0.418	6%	41%

Appendix C2 Crustal particulate Fe contributions

Crustal contributions of particulate Fe calculated with crustal ratios of 0.21 mol Fe/mol Al and 10 mol Fe/mol Ti. Crustal contributions exceeding 100% are highlighted in bold font.

Station	Depth [m]	labile Fe/Al [mol mol^{-1}]	labile Fe/Ti [mol mol^{-1}]	% crustal labile Fe Al	% crustal labile Fe Ti	refractory Fe/Al [mol mol^{-1}]	refractory Fe/Ti [mol mol^{-1}]	% crustal refractory Fe Al	% crustal refractory Fe Ti	total Fe/Al [mol mol^{-1}]	total Fe/Ti [mol mol^{-1}]	% crustal total Fe Al	% crustal total Fe Ti
33	768	0.696	35.520	30%	28%	0.258	5.597	81%	**179%**	0.322	7.603	65%	**132%**
	690	0.637	43.830	33%	23%	0.276	5.443	76%	**184%**	0.325	7.105	65%	**141%**
	592	0.627	52.395	33%	19%	0.280	5.623	75%	**178%**	0.324	7.192	65%	**139%**
	443	0.684	31.266	31%	32%	0.269	5.874	78%	**170%**	0.323	7.589	65%	**132%**
	195	0.610	30.294	34%	33%	0.282	6.262	74%	**160%**	0.338	8.277	62%	**121%**
	146	0.594	36.385	35%	27%	0.267	5.319	79%	**188%**	0.315	6.986	67%	**143%**
	97	0.553	75.698	38%	13%	0.253	5.467	83%	**183%**	0.289	6.944	73%	**144%**
	72	0.448	133.858	47%	7%	0.301	4.450	70%	**225%**	0.318	5.278	66%	**189%**
	44	0.442	111.006	48%	9%	0.354	4.990	59%	**200%**	0.363	5.609	58%	**178%**
	19	0.735	78.688	29%	13%	0.421	4.021	50%	**249%**	0.479	5.515	44%	**181%**
	10	0.607	143.901	35%	7%	0.384	4.082	55%	**245%**	0.414	5.044	51%	**198%**
34	542	0.689	30.841	30%	32%	0.276	6.147	76%	**163%**	0.336	8.078	62%	**124%**
	492	0.685	48.129	31%	21%	0.293	6.700	72%	**149%**	0.338	8.398	62%	**119%**
	393	0.614	33.761	34%	30%	0.281	6.352	75%	**157%**	0.324	7.910	65%	**126%**
	295	0.612	27.438	34%	36%	0.257	5.916	82%	**169%**	0.310	7.674	68%	**130%**
	186	0.700	50.530	30%	20%	0.256	5.299	82%	**189%**	0.303	6.795	69%	**147%**
	156	0.660	56.638	32%	18%	0.244	5.727	86%	**175%**	0.281	7.035	75%	**142%**
	97	0.554	72.533	38%	14%	0.239	5.774	88%	**173%**	0.262	6.720	80%	**149%**
	72	0.731	74.413	29%	13%	0.266	4.725	79%	**212%**	0.301	5.713	70%	**175%**
	48	0.621	52.105	34%	19%	0.245	5.381	86%	**186%**	0.275	6.429	76%	**156%**
	20	0.684	58.691	31%	17%	0.248	4.099	85%	**244%**	0.283	5.014	74%	**199%**
	9	1.140	170.042	18%	6%	0.629	15.357	33%	**65%**	0.663	17.176	32%	**58%**
36	295	0.605	35.646	35%	28%	0.266	5.985	79%	**167%**	0.308	7.511	68%	**133%**
	245	0.641	32.120	33%	31%	0.263	6.060	80%	**165%**	0.317	7.906	66%	**126%**
	196	0.594	32.060	35%	31%	0.260	5.481	81%	**182%**	0.308	7.120	68%	**140%**
	146	0.633	96.954	33%	10%	0.221	5.491	95%	**182%**	0.248	6.526	85%	**153%**
	72	0.648	90.162	32%	11%	0.228	5.655	92%	**177%**	0.262	6.953	80%	**144%**
	32	0.619	60.085	34%	17%	0.237	5.781	89%	**173%**	0.271	7.089	77%	**141%**
	9	0.618	64.400	34%	16%	0.226	5.732	93%	**174%**	0.258	7.012	81%	**143%**
42	769	0.648	41.008	32%	24%	0.238	5.589	88%	**179%**	0.284	7.152	74%	**140%**
	690	0.648	34.059	32%	29%	0.250	5.709	84%	**175%**	0.299	7.353	70%	**136%**
	641	0.610	29.875	34%	33%	0.251	5.915	84%	**169%**	0.295	7.452	71%	**134%**
	542	0.626	31.330	34%	32%	0.265	5.762	79%	**174%**	0.312	7.311	67%	**137%**
	344	0.649	36.169	32%	28%	0.239	5.257	88%	**190%**	0.288	6.816	73%	**147%**
	245	0.720	67.954	29%	15%	0.188	5.408	**112%**	**185%**	0.220	6.618	95%	**151%**
	97	0.640	53.102	33%	19%	0.201	5.265	**104%**	**190%**	0.239	6.651	88%	**150%**
	72	0.677	50.544	31%	20%	0.201	5.211	**104%**	**192%**	0.239	6.522	88%	**153%**
	47	0.579	77.981	36%	13%	0.217	5.665	97%	**177%**	0.244	6.763	86%	**148%**

Station	Depth [m]	labile Fe/Al [mol mol^{-1}]	labile Fe/Ti [mol mol^{-1}]	% crustal labile Fe Al	% crustal labile Fe Ti	refractory Fe/Al [mol mol^{-1}]	refractory Fe/Ti [mol mol^{-1}]	% crustal refractory Fe Al	% crustal refractory Fe Ti	total Fe/Al [mol mol^{-1}]	total Fe/Ti [mol mol^{-1}]	% crustal total Fe Al	% crustal total Fe Ti
42	18	0.639	70.564	33%	14%	0.221	5.056	95%	**198%**	0.250	6.055	84%	**165%**
	11	0.525	81.052	40%	12%	0.231	5.834	91%	**171%**	0.251	6.716	84%	**149%**
45	507	0.603	45.413	35%	22%	0.269	6.446	78%	**155%**	0.305	7.922	69%	**126%**
	442	0.652	31.741	32%	32%	0.285	6.219	74%	**161%**	0.332	7.789	63%	**128%**
	394	0.641	30.560	33%	33%	0.287	6.111	73%	**164%**	0.331	7.548	64%	**132%**
	345	0.620	18.479	34%	54%	0.316	4.445	67%	**225%**	0.357	5.415	59%	**185%**
	235	0.695	34.549	30%	29%	0.255	5.993	82%	**167%**	0.298	7.384	70%	**135%**
	176	0.715	49.184	29%	20%	0.269	1.103	78%	**907%**	0.311	1.404	67%	**712%**
	97	0.651	60.522	32%	17%	0.245	4.916	86%	**203%**	0.290	6.354	72%	**157%**
	73	0.486	67.414	43%	15%	0.256	4.986	82%	**201%**	0.284	6.180	74%	**162%**
	47	0.656	194.527	32%	5%	0.338	3.009	62%	**332%**	0.383	3.965	55%	**252%**
	15	0.829	100.125	25%	10%	0.342	3.453	61%	**290%**	0.404	4.609	52%	**217%**
	10	0.930	82.389	23%	12%	0.305	4.479	69%	**223%**	0.350	5.467	60%	**183%**
48	592	0.588	34.373	36%	29%	0.267	6.911	79%	**145%**	0.305	8.479	69%	**118%**
	444	0.760	34.000	28%	29%	0.254	6.656	83%	**150%**	0.305	8.346	69%	**120%**
	231	0.656	36.803	32%	27%	0.258	5.928	82%	**169%**	0.305	7.552	69%	**132%**
	96	0.640	62.953	33%	16%	0.238	6.409	88%	**156%**	0.277	8.004	76%	**125%**
	47	0.599	55.618	35%	18%	0.251	5.514	84%	**181%**	0.284	6.704	74%	**149%**
	10	0.440	24.281	48%	41%	0.453	4.939	46%	**202%**	0.451	5.469	47%	**183%**
49	572	0.527	50.558	40%	20%	0.251	6.560	84%	**152%**	0.278	7.833	75%	**128%**
	494	0.689	53.930	30%	19%	0.276	6.070	76%	**165%**	0.323	7.735	65%	**129%**
	443	0.621	34.277	34%	29%	0.272	6.280	77%	**159%**	0.311	7.712	67%	**130%**
	314	0.260	50.861	81%	20%	0.266	6.296	79%	**159%**	0.265	7.548	79%	**132%**
	216	0.667	51.404	31%	19%	0.233	6.155	90%	**162%**	0.269	7.522	78%	**133%**
	156	0.740	80.509	28%	12%	0.239	5.915	88%	**169%**	0.275	7.208	76%	**139%**
	97	0.138	93.372	**153%**	11%	0.251	5.222	84%	**191%**	0.219	6.254	96%	**160%**
	69	0.490	109.489	43%	9%	0.264	5.320	79%	**188%**	0.284	6.233	74%	**160%**
	38	0.882	73.677	24%	14%	0.209	2.474	**101%**	**404%**	0.261	3.311	81%	**302%**
	21	0.235	87.878	89%	11%	0.533	2.804	39%	**357%**	0.426	3.466	49%	**288%**
	10	0.501	30.250	42%	33%	0.365	2.288	57%	**437%**	0.386	2.806	54%	**356%**
52	483	0.516	37.420	41%	27%	0.317	6.615	66%	**151%**	0.339	7.671	62%	**130%**
	394	0.554	49.090	38%	20%	0.328	6.451	64%	**155%**	0.355	7.687	59%	**130%**
	295	0.813	62.241	26%	16%	0.352	4.929	60%	**203%**	0.400	6.110	53%	**164%**
	146	0.868	102.666	24%	10%	0.338	5.071	62%	**197%**	0.386	6.307	54%	**159%**
	97	0.873	96.138	24%	10%	0.326	4.084	65%	**245%**	0.385	5.345	55%	**187%**
	57	0.980	103.688	21%	10%	0.334	3.463	63%	**289%**	0.404	4.631	52%	**216%**
	25	0.596	62.903	35%	16%	0.427	2.466	49%	**406%**	0.465	3.405	45%	**294%**
	9	0.876	61.900	24%	16%	0.439	3.505	48%	**285%**	0.483	4.237	43%	**236%**
53	1015	1.234	104.269	17%	10%	0.406	1.822	52%	**549%**	0.512	2.614	41%	**383%**
	789	1.227	119.935	17%	8%	0.344	1.437	61%	**696%**	0.485	2.383	43%	**420%**
	690	1.301	101.709	16%	10%	0.362	2.118	58%	**472%**	0.502	3.407	42%	**293%**
	542	1.241	120.010	17%	8%	0.242	1.633	87%	**612%**	0.339	2.518	62%	**397%**
	394	1.052	114.670	20%	9%	0.351	1.695	60%	**590%**	0.459	2.596	46%	**385%**

Station	Depth [m]	labile Fe/Al [mol mol^{-1}]	labile Fe/Ti [mol mol^{-1}]	% crustal labile Fe Al	% crustal labile Fe Ti	refractory Fe/Al [mol mol^{-1}]	refractory Fe/Ti [mol mol^{-1}]	% crustal refractory Fe Al	% crustal refractory Fe Ti	total Fe/Al [mol mol^{-1}]	total Fe/Ti [mol mol^{-1}]	% crustal total Fe Al	% crustal total Fe Ti
53	196	0.877	149.705	24%	7%	0.296	2.794	71%	**358%**	0.373	4.039	56%	**248%**
	97	0.771	193.648	27%	5%	0.484	1.893	43%	**528%**	0.555	2.863	38%	**349%**
	67	0.694	206.010	30%	5%	0.405	2.481	52%	**403%**	0.471	3.710	45%	**270%**
	37	1.096	142.188	19%	7%	0.403	2.579	52%	**388%**	0.511	3.839	41%	**261%**
	24	0.489	89.374	43%	11%	0.627	2.167	33%	**461%**	0.588	2.817	36%	**355%**
	10	0.874	116.749	24%	9%	0.418	2.716	50%	**368%**	0.484	3.639	43%	**275%**